HHS Public Access

Author manuscript

Nat Med. Author manuscript; available in PMC 2018 September 12.

Published in final edited form as:

Nat Med. 2018 May ; 24(4): 438–449. doi:10.1038/nm.4491.

Dentate granule cell recruitment of feedforward inhibition governs engram maintenance and remote memory generalization

Nannan Guo[1,2,3], **Marta E. Soden**[5,6], **Charlotte Herber**[1,2], **Michael TaeWoo Kim**[1,2,3], **Antoine Besnard**[1,2,3], **Paoyan Lin**[1,2,3], **Xiang Ma**[7,8], **Constance L. Cepko**[7,8], **Larry S. Zweifel**[5,6], and **Amar Sahay**[*,1,2,3,4]

[1]Center for Regenerative Medicine, Massachusetts General Hospital, Boston, MA 02114, USA

[2]Harvard Stem Cell Institute, Cambridge, MA 02138, USA

[3]Department of Psychiatry, Massachusetts General Hospital, Harvard Medical School, Boston, MA 02114, USA

[4]BROAD Institute of Harvard and MIT, Cambridge, MA 02142

[5]Department of Pharmacology, University of Washington, Seattle, WA, USA

[6]Department of Psychiatry and Behavioural Sciences, University of Washington, Seattle, WA, USA

[7]Howard Hughes Medical Institute

[8]Department of Genetics, Harvard Medical School, Boston, MA

Abstract

Memories become less precise and generalize over time as memory traces re-organize in hippocampal-cortical networks. Increased time-dependent loss of memory precision characterizes overgeneralization of fear in post-traumatic stress disorder (PTSD) and age-related cognitive impairments. In the hippocampal dentate gyrus (DG), memories are thought to be encoded by so-called “engram-bearing” dentate granule cells (eDGCs). Here we show using rodents that contextual fear conditioning increases connectivity between eDGCs and inhibitory interneurons in the downstream hippocampal CA3 region. We identify actin-binding LIM protein 3 (abLIM3) as a mossy fiber terminal localized cytoskeletal factor, whose levels decrease upon learning. Downregulation of abLIM3 in DGCs was sufficient to increase connectivity with CA3 stratum lucidum interneurons (SLINs), promote parvalbumin (PV) SLIN activation, enhance feed-forward

[*]Correspondence and requests for materials should be addressed to asahay@mgh.harvard.edu.

Author contributions

N.G, M.E.S, C.H, M.T.K, P.L., and A.B. performed experiments. X.M and C.L.C. contributed reagents. M.E.S and L.S.Z contributed to slice electrophysiology experiments and interpretation. A.S and N.G co-developed the concept, analyzed data and wrote the manuscript. A.S conceived the project and supervised all aspects of the project.

Competing Financial Interests Statement

The authors declare competing financial interests. A.S and N.G are named co-inventors on patent application relating to this study.

inhibition onto CA3, and maintain a fear memory engram in the dentate gyrus (DG) over time. Furthermore, abLIM3 downregulation in DGCs conferred conditioned context-specific reactivation of memory traces in hippocampal-cortical and amygdalar networks and decreased fear memory generalization at remote time points. Consistent with age-related hyperactivity of CA3, learning failed to increase DGC-SLIN connectivity in 17 month-old mice, whereas abLIM3 downregulation was sufficient to restore DGC-SLIN connectivity, increase PV-SLIN activation and improve remote memory precision. These studies exemplify a connectivity-based strategy targeting a molecular brake of feedforward inhibition in DG-CA3 that may be harnessed to decrease time-dependent memory generalization in PTSD and improve memory precision in aging.

Introduction

Memories become generalized over time as their details are lost. Time-dependent generalization of traumatic memories results in expression of fear in neutral environments at remote time points, a feature of post-traumatic stress disorder (PTSD) that is captured in numerous animal studies[1–7]. Memory imprecision also characterizes mild cognitive impairment and episodic memory dysfunction during aging[8,9]. Recent studies have begun to identify circuit mechanisms underlying memory precision and generalization of recent memories[5,10–15]. In contrast, we know much less about the circuit mechanisms governing the time-dependent erosion of details that gradually lead to generalization of remote memories[1]. Bridging this gap will edify new strategies to preserve memory precision in aging and curb time-dependent fear generalization in PTSD.

Unlike generalization of recent memories, the generalization of remote memories is thought to reflect time-dependent re-organization of memory traces in hippocampal-cortical networks[16–18]. Growing evidence supports a continuous role for the hippocampus in maintaining the specificity of memories over time through hippocampal-cortical interactions underlying memory consolidation[17,19–23]. These observations together with hippocampal index theory[5,21,22] suggest that new memories presumably encoded in hippocampal eDGCs[24,25] may serve as indexes for stabilization of cognate cortical representations[5,16,21,22]. Consistent with this idea, genetic disruption of engram bearing DGCs (eDGCs) during learning impaired early maturation of cortical engram cells[25]. However, the circuit mechanisms by which eDGCs connectivity dictate time-dependent re-organization of memory traces in hippocampal-cortical networks and govern remote memory generalization remain poorly understood.

DGC connectivity with stratum lucidum interneurons (SLINs) has been suggested to govern precision of recent memories[11]. Mossy fiber terminals (MFTs) form excitatory synapses onto thorny excrescence-like dendritic spines of CA3 neurons and filopodia emanating from MFTs that contact SLINs are thought to mediate feed-forward inhibition onto CA3[26–28]. DGC recruitment of inhibition onto CA3 is thought to determine the temporal window of spiking of CA3 neurons and potentially, dictate CA3 activation patterns[28,29]. Interestingly, MFT filopodia number is inversely correlated with fear generalization over time[11]. Mice lacking the brain-wide expressed cytoskeletal factor (Adducin 2) exhibit impaired synaptic

plasticity and learning and memory, failure to increase DGC-SLIN connectivity following learning, and increased generalization of a fear memory one day after conditioning[11,30,31] that was rescued by re-expression of Adducin 2 in the DG. CA3 outputs and parvalbumin expressing interneurons (PV INs) have been suggested to promote hippocampal–cortical communication through modulation of sharp wave ripples[32–37]. Based on these findings, we hypothesized that DGC recruitment of inhibition onto CA3 maintains the DG engram over time and this in turn, dictates time-dependent re-organization of memory traces in hippocampal-cortical networks and decreases remote memory generalization. Critical to testing this hypothesis is identifying a molecular control by which DGC recruitment of inhibition onto CA3 maybe acutely and selectively enhanced.

Evidence from studies in rodents, non-human primates and humans suggests that aging is associated with CA3 hyperexcitability, hyperactivity and inflexible remapping[38–42]. Decreased DGC recruitment of inhibition onto CA3[42], decline in number of SLINs[41], decreased DGC spine density[43], and increased intrinsic CA3 excitability[40] may all contribute to age-related changes in CA3. Whether DGC-SLIN connectivity is altered in aging and whether enhancing DGC recruitment of inhibition is sufficient to enhance memory precision in aging is not known.

RESULTS

abLIM3 is a learning-regulated molecular brake of DGC-SLIN connectivity

We first examined DGC-SLIN connectivity of engram bearing DGCs (eDGCs) at recent and remote time points after contextual fear conditioning. Using 3 month-old cfos-tTA:tetO-Tau-lacZ transgenic mice[44] in combination with a teto-Tau-lacZ reporter line to indelibly label memory engrams by removal of doxycycline from the animal's diet during conditioning (Fig. 1a), we found that eDGCs encoding the fear conditioned context had significantly greater number of MFT filopodia than non-tagged DGCs one day post training, without affecting the proportion of MFT filopodial contacts with PV SLINs (Supplementary Fig.1b). However, the number of MFT filopodia of eDGCs decreased to levels of non-tagged ("non-engram") DGCs at the remote time point, day 16 (Fig. 1b), when memory becomes imprecise and is generalized[2,3].

To causally assess how DGC recruitment of inhibition affects engram properties, we sought to identify a selective molecular regulator of DGC-SLIN connectivity. We examined brain-wide expression patterns of putative targets of Kruppel-like factor 9, a transcriptional regulator of DGC maturation[45] and identified *Ablim3* as a candidate factor[46,47]. *Ablim3* is highly expressed in DGCs and is negligibly expressed in CA subfields (Fig. 1c, http://hipposeq.janelia.org/full/t1/F64339A8-AF50-11E7-AD92-C0A401797C37/). Outside of the hippocampus, *Ablim3* is enriched in granule cells of the main olfactory bulb and cerebellum (Allen Brain Atlas, http://mouse.brain-map.org/experiment/show/69626582)[47]. Immunohistochemistry in adult mouse brain sections revealed that abLIM3 is absent from CA1-CA3 subregions and molecular layers of the hippocampus, but is exclusively localized to MFTs (labeled with vesicular glutamate transporter 1, VGLUT1, Fig. 1c-d, Supplementary Fig.1a). Within MFTs, abLIM3 is absent from active zones (labeled by bassoon immunoreactivity) but is localized to puncta adherens junctions (PAJs), sites of

MFT stabilization on dendritic shafts of CA3 neurons, as indicated by overlap with zona occludens-1, ZO-1, a marker of PAJs (Fig. 1d, j, Supplementary Fig.1a). Western blot analysis of abLIM3 levels in hippocampus of naïve and contextual fear-conditioned (training) mice revealed that abLIM3 levels are decreased following learning compared with naïve mice (Fig.1e, Supplementary Fig.1c and Supplementary Fig. 11). abLIM3 levels, albeit low, in CA1 remained unchanged following learning (Supplementary Fig.1d and Supplementary Fig. 11). Based on these observations and evidence supporting a role for abLIM3 in stabilizing branched F-actin in lamellipodia[48,49], we predicted that abLIM3 levels in MFTs constrain generation of MFT filopodial contacts with SLINs.

To determine whether abLIM3 functions as a molecular brake of DGC-SLIN connectivity, we engineered lentiviruses expressing shRNAs to downregulate abLIM3 *in vitro* (Supplementary Fig.2a). Stereotactic injections of lentiviral shRNA #46 into the DG significantly downregulated *Ablim3* transcripts in DGCs (Supplementary Fig.3a-b) and decreased abLIM3 in MFTs (Fig. 1f). Lentiviral infection primarily targets mature DGCs as fewer than 4% of GFP-expressing cells also expressed the marker of immature adult-born DGCs, doublecortin (DCX) (Supplementary Fig.3c-d). Lentiviral downregulation of abLIM3 in DGCs using two different shRNAs (shRNA#46 or shRNA#47) increased the number of filopodia per MFT, but did not affect MFT filopodial length, MFT size, or dendritic spine density of DGCs (Fig. 1g, Supplementary Fig.2b-c). abLIM3 downregulation in DGCs did not affect the proportion of VGLUT1+ MFT filopodial contacts with PV or somatostatin (SST) SLINs (Fig.1h, Supplementary Fig.2d). Stereotaxic injection of the anterograde tracer, vesicular stomatitis virus expressing GFP[50], into DGCs following abLIM3 downregulation resulted in increased transsynaptic labeling of GABA and PV SLINs at 2 days (Fig.1i), but not immediately (day 0), following injection (Supplementary Fig.2f). abLIM3 downregulation in DGCs did not affect the expression of GABA or PV in the stratum lucidum (Supplementary Fig.2e). Together, these data demonstrate that abLIM3 is a molecular brake of DGC-SLIN connectivity and that decreasing abLIM3 levels in DGCs of adult mice mimics learning induced increase in DGC-SLIN connectivity (Fig. 1j).

abLIM3 downregulation in DGCs promotes DGC recruitment of inhibition onto CA3

Although it is assumed that DGC-SLIN connectivity mediates GABAergic inhibition onto CA3[11], evidence linking acute modulation of DGC-SLIN connectivity in adult mice with electrophysiological changes in inhibition onto CA3 is conspicuously absent[28]. Therefore, we asked whether increasing DGC-SLIN connectivity by abLIM3 downregulation translated into physiological changes in excitatory inputs onto PV INs and increased GABAergic inhibition onto CA3. Characterization of mice in which PV SLINs were genetically labeled with tdTomato (PV-Cre:Ai14 mice) revealed that 90% of tdTomato+ cells also expressed PV (Fig. 2a-b). Next, we performed whole-cell recordings from tdTomato-expressing PV SLINs and CA3 pyramidal neurons in slices obtained from PV-Cre:Ai14 mice following lentiviral injections of shRNA and shNT constructs into the DG (Fig. 2c). Downregulating abLIM3 in DGCs increased frequency of miniature excitatory postsynaptic currents (mEPSCs) in PV SLINs (Fig. 2d, g) consistent with increased numbers of VGLUT1+ MFT filopodial contacts onto PV SLINs (Fig. 1g, h). Interestingly, we noted a decrease in amplitude of mEPSCs in PV SLINs suggestive of potential homeostatic changes in response to the increased

excitatory drive onto these cells (Fig. 2d, g). Recordings from CA3 pyramidal neurons revealed an increase in frequency, but not amplitude, of miniature inhibitory postsynaptic currents (mIPSCs) (Fig. 2e, g). Consistent with increased mIPSCs in CA3 neurons, increasing mossy fiber excitatory drive onto PV SLINs significantly enhanced the number of PV-positive puncta density in the CA3 pyramidal layer (Fig.2h). Additionally, amplitude of miniature excitatory postsynaptic currents (mEPSCs) in CA3 neurons was decreased with no effect on mEPSC frequency (Fig. 2f, g).

To determine the net effect of these synaptic changes and whether abLIM3 levels in DGCs dictate feed-forward inhibition onto CA3, we co-injected rAAV$_5$-CamKIIα Channelrhodopsin (ChR2) and lentiviruses expressing shRNA or shNT into DG and performed whole cell recordings in CA3 pyramidal neurons in hippocampal slices following blue light stimulation (Fig. 3a). Decreasing abLIM3 level in DGCs resulted in greater recruitment of feed-forward inhibition onto CA3 neurons as evidenced in a significant decrease in the excitation-inhibition ratio. This effect was driven by an increase in evoked IPSCs in CA3 neurons (Fig. 3a-b). Bath application of DCG-IV, a group II metabotropic glutamate receptor agonist that selectively blocks evoked MFT release[28,51], to hippocampal slices abolished evoked inhibitory and excitatory responses in CA3 (Fig. 3c).

abLIM3 downregulation in DGCs maintains engram in DG and constrains re-activation of remote memory traces in CA3-CA1-ACC and BLA networks

Because DGC-SLIN connectivity of eDGCs, is transiently increased relative to non-engram bearing cells following learning and returns to baseline at remote timepoints when memory is generalized, we asked if enhancing DGC-PV SLIN connectivity promoted maintenance of a fear conditioned context (context A) engram in the DG. We injected AAV$_9$ tetO-channelrhodopsin (ChR2)-enhanced yellow fluorescent protein (eYFP) expressing virus and shRNA-GFP or non-target shRNA (shNT-GFP) expressing lentivirus into the DG of cfos-tTA[44,52] transgenic mice prior to contextual fear conditioning in context A (Fig. 4a). Following tagging of context A ensembles with ChR2-eYFP, we activated the context A neuronal ensemble in a neutral, distinct context C at day 2 and day 10 by shining blue light above the DG in both groups of mice (Fig. 4b, c). Both groups exhibited comparable levels of light-induced freezing at day 2 suggesting comparable numbers of tagged and activated DGCs in both groups of mice. However, at day 10, only the shRNA group permitted optogenetic dependent artificial recall of the contextual fear memory (Fig. 4c). Blue light did not elicit freezing behavior in context C in non-conditioned, context A-exposed mice (Fig. 4b-c). Examination of eDGCs revealed a ~50% reduction in number of tagged ChR2-eYFP expressing eDGCs (Supplementary Fig.4a)[52] potentially, explaining the lack of induction of freezing behavior by blue light in controls[25]. Injection of AAV$_9$ tetO-ChR2-mCherry expressing virus and shRNA-GFP or non-target shRNA (shNT-GFP) expressing lentivirus into the DG of cfos-tTA mice revealed that abLIM3 downregulation in DGCs does not affect ChR2 stability (Supplementary Fig.4b-c). Thus, despite decreased expression of the ChR2 tag over time and the time-dependent reduction in dendritic spine density of eDGCs[25], increasing DGC recruitment of inhibition by abLIM3 downregulation sufficed to permit engram activation at a remote timepoint.

Next, we asked whether enhancing DGC recruitment of feedforward inhibition by abLIM3 downregulation affects context specific re-activation of memory traces in hippocampal-cortical networks over time. We stereotactically injected lentiviral shRNA-GFP or shNT-GFP into DG of Tet-Tag mice harboring a knock-in H2BmCherry reporter allele to indelibly label cells activated during conditioning to context A (Supplementary Fig.4d-e). Reactivation of the DG ensemble in context A decreased overtime, indicating that engram may become gradually silenced with time as the memory generalizes (Fig. 4d-e). Both shRNA and shNT injected mice exhibited equivalent levels of reactivation of context A ensembles in DG when mice were re-exposed to context A and context C at immediate (day 1 post training) and remote timepoints (day 16) (Fig. 4e, Supplementary Fig.6a). However, abLIM3 downregulation in DGCs significantly decreased reactivation of context A ensembles in CA3 when mice were exposed to the neutral context C at remote, but not immediate, timepoint (Fig. 4e, Supplementary Fig.6b). RGS14 immunostaining was performed to exclude CA2 cells from CA3 quantification (Supplementary Fig.6b). Consistent with these observations, using Tet-tag mice with transgenic tetO-H2B-GFP reporter alleles we found that abLIM3 downregulation decreased reactivation of context A ensembles in CA3 (Supplementary Fig.5a) and CA1 when mice were placed in a neutral context C at the remote timepoint, day 16 (Fig. 4f-g, Supplementary Fig.6c). Both groups of mice (carrying tetO-H2B-GFP or H2BmCherry reporter alleles) exhibited comparable numbers of labeled cells (Supplementary Fig.5b-d) and similar percentages of chance overlap (Supplementary Fig.5e) in DG, CA3 and CA1.

The anterior cingulate cortex (ACC) is a storage site of remote memories[17,25,53]. To determine whether abLIM3 downregulation in DGCs also modulated re-activation of context A ensembles in the ACC, we used cfos-tTA transgenic mice in combination with a tetO-H2B-GFP reporter line to indelibly tag context A cortical ensembles (Fig. 4f-g). Downregulation of abLIM3 in DG of these mice increased reactivation of context A ensemble in Cg1, but not Cg2, fields of the ACC following exposure to context A at remote timepoint (Fig. 4g, Supplementary Fig.5a, Supplementary Fig.6e-f). Furthermore, reactivation of context A ensemble in Cg1 following exposure to context C was decreased (Fig. 4g, Supplementary Fig.6e-f). Both groups of mice exhibited comparable numbers of labeled cells in ACC and similar percentages of chance overlap (Supplementary Fig.5b, d, e).

The BLA acts downstream of the hippocampus and prefrontal cortex to govern expression of fear[54–56]. Therefore, we examined activation dynamics of H2B-GFP tagged context A ensemble in the BLA over time and following abLIM3 downregulation in DGCs (Supplementary Fig.6d). Interestingly, we found a time-dependent increase in reactivation of the H2B-GFP tagged context A ensemble in the BLA following exposure to neutral context (Day 1 vs. Day 16, shNT group, Fig. 4f-g). Remarkably, abLIM3 downregulation in DGCs constrained this time-dependent generalization of the fear memory trace in the BLA (Day 1 vs. Day 16, shRNA group, Fig. 4f-g). Both groups of mice exhibited comparable numbers of labeled cells in BLA and similar percentages of chance overlap (Supplementary Fig.5b, d, e).

abLIM3 downregulation in DGCs decreases remote memory generalization

Next, we asked whether abLIM3 downregulation in the DG decreases generalization of remote fear memories. We stereotactically injected shRNA-GFP or shNT-GFP expressing lentiviruses into DG and 2 weeks later, mice were conditioned to 3 footshocks in context A and then exposed to context A and a neutral, distinct context C in a counterbalanced manner 1 day, 10 days and 16 days post training. abLIM3 downregulation in DG significantly decreased levels of freezing in context C and improved discrimination between contexts A and C at remote (significant effect on day 16, trend on day 10), but not recent (day 1), time points (Fig. 5a-d). abLIM3 downregulation in the DG resulted in increased sparseness of activity in CA3 following exposure to context C, but not in the homecage group, at the remote timepoint (Fig. 5e-g) consistent with the decreased reactivation of context A ensembles in CA3 when mice were exposed to the neutral context C at remote time point (Fig. 4e). Using a separate cohort of mice that was not exposed to context C until day 16, we found that abLIM3 downregulation in DGCs significantly decreased levels of freezing in context C at the remote, but not recent, timepoint (Fig. 5h-k). These mice showed a trend towards better discrimination between contexts A and C at day 16 (Fig.5k) Interestingly, and as seen in adult mice, abLIM3 downregulation in DGCs increased activation of PV, but not SST, SLINs when assessed at the remote timepoint (Supplementary Fig.8a-e). abLIM3 downregulation in DGCs did not affect activity of DG (Supplementary Fig.7a-b), contextual fear acquisition, locomotor activity, behavioral measures of anxiety or behavior in the tail suspension test (Fig. 5b, i, Supplementary Fig.7c-g).

abLIM3 downregulation in DG of aged mice improves remote memory precision

Aging is associated with decreased feed-forward inhibition in DG-CA3 and CA3 hyperactivity[38–42]. To determine if DGC-PV SLIN connectivity decreases with aging, we injected DG of 17 months old mice with lentivirus expressing shNT-GFP and examined MFT filopodia (Fig. 6a). Aged mice exhibited decreased DGC dendritic spine density (unpaired t-test, shNT group, 3 month vs 17 month: $p=0.04$) and a modest reduction in number of MFT filopodia at baseline. However, aged mice were refractory to learning-induced increases in number of MFT filopodia that was seen in adult mice (Fig. 6b). Based on these observations, we asked whether we could harness abLIM3 to restore DGC-SLIN connectivity in aged mice. Injection of shRNA targeting abLIM3 into DG of aged mice profoundly increased the number of VGLUT+ MFT filopodial contacts with PV SLINs and the density of PV-positive puncta in the CA3 pyramidal cell layer, without affecting MFT size or DGC dendritic spine density (Fig. 6c-d, Supplementary Fig.9a-c). Stereotactic injection of vesicular stomatitis virus expressing GFP into DG of 17 months old mice resulted in increased anterograde transsynaptic labeling of GABA and PV SLINs in CA3 following abLIM3 downregulation in DGCs (Fig. 6e). abLIM3 downregulation in DGCs did not affect the expression of GABA or PV in CA3 (Supplementary Fig.9d)

We next sought to determine if increasing DGC-PV SLIN connectivity in aged mice by abLIM3 downregulation in DG is sufficient to improve precision of remote memories. Following abLIM3 downregulation in DG, 17-month-old mice exhibited better memory for conditioning context A at day 10 following training resulting in significantly higher discrimination between the conditioning context A and a distinct, neutral context C (Fig. 6f-

i). Further, at day 16 following training, aged mice with restored DGC-SLIN connectivity exhibited stronger memory for context A and increased activation of PV and CA3 pyramidal neurons, but not SST SLINs or DGCs following exposure to context A (Fig. 6j, k, Supplementary Fig.9e-g), which is consistent with the modest increase in reactivation of context A ensemble in CA3 when mice were exposed to the context A at remote time point (Fig. 4e, p=0.05). Increasing DGC-SLIN connectivity in aged mice by abLIM3 downregulation in DG did not affect locomotor activity but produced anxiolytic-like behavioral effects in the elevated plus maze and decreased immobility in the tail suspension test (Supplementary Fig.10).

DISCUSSION

Our studies causally link a mossy fiber terminal localized cytoskeletal factor, abLIM3, with DGC-SLIN connectivity, DGC recruitment of feedforward inhibition onto CA3, re-organization of remote memory traces in hippocampal-cortical-BLA networks and remote memory generalization.

abLIM3 belongs to the abLIM family that was originally characterized as regulators of growth cone motility in axon guidance[46]. abLIM3's role in stabilization of branched F-actin in lamellipodia[47–49] and its localization to PAJs, sites of structural stabilization of the MFT on the CA3 dendritic shaft, suggest that the molecular mechanisms underlying generation of growth cone-filopodia during development, that are notably distinct from those underlying dendritic filopodia[57], maybe re-used in controlling the generation of MFT filopodia in mature DGCs. The convergent elongation model of filopodial formation suggests a trade-off in growth cone lamellipodia versus filopodia during development[57,58]. Consistent with this model, retroviral downregulation of abLIM3 in 4 weeks, but not 8 weeks old, adult-born DGCs increased number of MFT filopodia and decreased MFT size (N.G and A.S, unpublished observations). abLIM3 downregulation in mature DGCs does not significantly affect MFT size presumably because the MFT is already stabilized onto the dendritic shaft of CA3. Based on these observations, we predict that factors regulating de-stabilization of branched F-actin networks in MFTs of mature DGCs may dictate the number of MFT filopodial contacts with SLINs to promote recruitment of inhibition onto CA3 in response to learning.

Although studies have begun to edify how afferent connectivity of eDGCs changes over time[25], much less is known about how efferent connectivity of eDGCs dictates engram properties. We found that learning induced a greater increase in eDGCs-SLIN connectivity than non-eDGCs and that eDGC-SLIN connectivity decreased over time as memory generalized. By virally harnessing abLIM3, we found that increasing DGC recruitment of inhibition onto CA3 permitted artificial recall of a memory trace by light stimulation of eDGCs at a remote timepoint that was otherwise not possible in controls. These observations suggest that maintaining eDGC-SLIN connectivity may, in turn, maintain the engram in the DG. Whether eDGCs recruit hippocampal-cortical replay mechanisms[59] or CA3 back-projections to maintain the engram remains to be addressed.

Increasing DGC recruitment of inhibition by abLIM3 downregulation in DGCs governed re-activation of memory traces of the conditioned context in CA3-CA1-ACC-BLA networks at remote timepoints. The decrease in context C induced reactivation of memory trace of the conditioned context in CA3, but not DG, at the remote timepoint implicates abLIM3 dependent changes in DGC-CA3 connectivity. We argue that constraining context specific CA3 reactivation dictates reactivation of the memory trace of the conditioned context in CA1, ACC and BLA. These findings generally support the transformative view of multiple trace theory of systems consolidation[18,19] and suggest that the memory of conditioned context is distributed over multiple traces in CA3, CA1, ACC and BLA that are linked or is one highly distributed trace. Our findings extend recent observations defining a role for the DG engram in early maturation of prefrontal cortical engram[25] to suggest that the DG engram may serve as a hippocampal index for time-dependent consolidation of cognate remote memory traces in the ACC[5,16,21,22] and govern reactivation dynamics in the BLA (Supplementary Fig. 12a-b)[55]. At the recent timepoint, intact input (dendritic spines) and output (DGC-SLIN) connectivity of eDGCs ensure context specific reactivation in CA3-CA1-ACC and BLA networks. With gradually silencing of the engram in DG and decrease in DGC-SLIN connectivity over time, context specific reactivation in CA3-CA1-ACC and BLA is impaired. However, increased DGC recruitment of inhibition onto CA3 continues to maintain DG engram and permit context specific reactivation in CA3-CA1-ACC-BLA networks (Supplementary Fig. 12a-b). Whether DG dependent modulation of ensemble reactivation and consolidation in BLA is independent of the ACC and is mediated by ventral CA1[56] remains to be determined.

Intriguingly, abLIM3 downregulation in DGCs increased PV, but not SST SLIN activation, despite increasing DGC connectivity with both these SLIN populations. Future studies dissecting SLIN microcircuitry may edify the basis of preferential recruitment of PV SLINs by DGCs[60]. Since increasing mossy fiber excitatory drive onto PV SLINs resulted in an increase in PV density in CA3, it is plausible that PV SLIN connectivity with downstream targets in CA3 and potentially, CA1 is also modified. These changes in PV SLIN connectivity over time may promote consolidation of remote memory cortical and subcortical traces through recruitment of replay mechanisms such as sharp-wave ripples[32–37] (Supplementary Fig. 12).

abLIM3 downregulation in DGCs decreased remote memory generalization. Because over generalization of remote traumatic memories characterizes PTSD, our findings suggest that efficient consolidation of a traumatic memory may decrease its generalization over time. It follows that therapeutic strategies that fail to completely block consolidation would exacerbate overgeneralization of fear. We suggest that mechanisms like pattern separation may help maintain the DG engram by decreasing interference between new and old similar engrams thereby promoting stabilization of cognate cortical and subcortical traces and decreasing remote memory generalization[5,22].

Converging evidence from studies in rodents, nonhuman primates and humans suggest a role for alterations in properties and functions of the DG-CA3 circuit in cognitive impairments in aging and MCI[9,38–42]. Although the fear conditioning training protocol used here did not permit detection of an age-related deficit in remote memory generalization[4], we observed a

profound failure in learning-induced increase in DGC-SLIN connectivity in aged mice. Importantly, abLIM3 downregulation in aged mice was sufficient to restore levels of DGC-SLIN connectivity, increase PV SLIN activation and improve remote memory precision. In light of these findings, it is notable that *Ablim3* expression is upregulated several fold in peripheral leukocytes of aged individuals who convert into amnestic subtype of MCI (WO2015184107 A1, Genetic markers for memory loss).

Excitation-inhibition imbalance in DG-CA3 may underlie memory impairments in aging and contribute to overgeneralization of fear in PTSD. By identifying a molecular regulator of DGC-SLIN connectivity, abLIM3, we show that increasing DGC recruitment of feedforward inhibition onto CA3 promotes engram maintenance in the DG and this in turn, governs reactivation of remote memory traces in hippocampal-cortical-BLA networks and decreases generalization of remote fear memories in adulthood and aging.

Data availability statement

Details of shRNA sequences and genetically modified mice can be found in the methods. This information is sufficient for interpretation and replication of the findings.

Methods

Online Content Methods, along with additional Extended Data display items (Supplementary figures 1-12, Supplementary Table 1), and Life Sciences Reporting Summary are available in the online version of the paper; references unique to these sections appear only in the online paper.

Subjects

All animals were handled and experiments were conducted in accordance with procedures approved by the Institutional Animal Care and Use Committees at the Massachusetts General Hospital and University of Washington, Seattle, in accordance with NIH guidelines. All mice were housed three-four per cage in a 12 hr (7:00 a.m. to 7:00 p.m.) light/dark colony room at 22°C–24°C with ad libitum access to food and water. Adult female C57Bl/6 mice (3-4 months old) were purchased from Jackson lab. Aged female C57Bl/6 mice (17-18 months old) were obtained from National Institute on Aging (NIA). The following mouse lines were obtained from Jackson Labs: cfos-tTA: tetO-taulacZ, tTA* (Stock No: 008344, Jackson labs), tetO-H2B-GFP (Stock No: 005104, Jackson labs), Col1a1-tetO-H2B-mCherry (Stock No: 014592, Jackson labs). TetTag mice were generated by crossing reporter mouse lines, tetO-H2B-GFP mouse line or tetO-H2B-mCherry mouse line, with mice that express tetracycline-trans-activator (tTA) protein under control of the c-fos promoter (Stock No: 008344, Jackson labs; outcrossed from tetO-lacZ, tTA*). c-fos-tTA mice also contain a transgene consisting of a c-fos promoter driving the expression of nuclear-localized 2-h half-life EGFP (shEGFP). All TetTag mice were maintained on a C57BL/6 background. Mice were bred and raised on doxycycline (dox) diet (40 mg kg^{-1} chow) to prevent any reporter expression prior to desired experimental labeling of ensembles. Dox diet was replaced with regular diet for 3 days to open the window for activity-dependent labeling of ensembles. Expression of reporter was shut off by

administration of dox diet immediately following desired labeling window. PV-Cre mice (stock No: 017320, Jackson labs) were bred with Ai14: tdTomato reporter mouse line (stock No: 007914, Jackson labs) to generate mice for viral injection and *in vitro* electrophysiological whole cell recordings.

Western blots analysis

To detect abLIM3 protein levels following learning, mice were subjected to contextual fear conditioning (Training, Figure 1e) and sacrificed by decapitation 1 h later to permit rapid dissection of hippocampus. Naïve control mice (Naïve, Figure 1e) were sacrificed and dissected directly from home cages. Hippocampi and CA3 subregions were dissected on Whatman paper soaked with ice-cold PBS and snap-frozen in liquid nitrogen immediately. Tissue was homogenized in radioimmunoprecipitation assay (RIPA) buffer (150mM NaCl, 0.1% sodium deoxycholate (SDS), 1% Triton X-100, 50mM Tris, pH 8.0) supplemented with 0.5 mM EDTA and Halt™Protease and Phosphatase Inhibitor Cocktail (Thermo Scientific, Waltham, MA). Homogenized samples were centrifuged at 12000 rpm for 20 minutes in 4°C. Protein concentrations were determined from supernatant by Pierce™ BCA Protein Assay Kit (Thermo Scientific, Waltham, MA). Diluted samples were supplemented with SDS sample buffer (2% SDS, 10% glycerol, 0.1M dithiothreitol, 0.01% bromophenol-blue, 62.5mM Tris, pH 6.8) and boiled at 95°C for 5 minutes. Proteins (40 μg) were resolved in 8% SDS-polyacrylamide gels by electrophoresis and transferred to PVDF membranes (Bio-Rad Laboratories, Hercules, CA) by electroblotting. To prevent non-specific binding, membranes were blocked with 3% dry milk in TBS-T (150mM NaCl, 20 mM Tris, 0.1% Tween-20) for 2 hours at room temperature. Membranes were incubated in primary antibodies, rabbit anti-abLIM3 (1:500, Abcam, ab129480) and mouse anti-GAPDH (1:2000, Millipore, MAB374, Billerica, MA), overnight at 4°C. Membranes were incubated in secondary antibodies, goat anti-rabbit HRP conjugate (1:5000, Bio-Rad Laboratories, 170-5046, Hercules, CA) and goat anti-mouse HRP conjugate (1:5000, Bio-Rad Laboratories, 170-5047, Hercules, CA), for 2 hours at room temperature. Membranes were imaged using the ChemiDoc™ XRS+ System. Images were analyzed using ImageJ using pixel intensities. For each membrane, relative densities of abLIM3 were calculated using each lane's corresponding GAPDH intensities.

Validation of shRNAs

shRNA lentiviral vectors were obtained from Sigma Mission library (Sigma-Aldrich). Five shRNAs targeting mouse abLIM3 (Cat. No.: SHCLNG-NM_198649) were verified. Lentiviral vector expressing Non-Mammalian non-target shRNA (SHC002) was used as a negative control. To validate efficiency of the shRNAs, each lentiviral shRNA vector was co-transfected with plasmids encoding HA-tagged full-length mouse abLIM3 and HA-tagged GFP into 293T cells. Cell lysates were subsequently prepared for western blot analysis of abLIM3 and GFP expression using mouse anti-abLIM3 antibody (Abcam, ab67721) and chicken anti-GFP antibody (Abcam, ab13970). β-actin (Abcam, ab8227) was used as a loading control. The shRNA sequences are as follows:

TRCN0000099545 (abLIM3):

CCGGCGCAGTATAATCCTCTTGTATCTCGAGATACAAGAGGATTATACTGCG TTTTTG;

TRCN0000099546 (abLIM3):

CCGGGCCTTTCCCTATTGGAGATAACTCGAGTTATCTCCAATAGGGAAAGGC TTTTTG;

TRCN0000099547 (abLIM3):

CCGGGTGGATAATGAGATCCTTAATCTCGAGATTAAGGATCTCATTATCCAC TTTTTG;

TRCN0000099548 (abLIM3):

CCGGGCGGACATCTGAAACTTCCATCTCGAGATGGAAGTTTCAGATGTCCG CTTTTTG;

TRCN0000099549 (abLIM3):

CCGGCTGGAAGAGGAACGAACTGAACTCGAGTTCAGTTCGTTCCTCTTCC AGTTTTTG;

Viral constructs

Non-target control shRNA (shNT) and validated shRNAs (shRNA#46 and shRNA#47) against abLIM3 were cloned into pLLX-shRNA lentiviral vector under the control of U6 promoter as previously described[61]. The pLLX-shRNA vector also contains a second expression cassette in which GFP is expressed from the ubiquitin promoter that allows the monitoring of transfection and infection efficiency. Lentiviral stock solutions (5-8 × 10^7 unit/ml) were prepared by cotransfection of pLLX-shRNA lentiviral vector and packaging plasmids into HEK293T cells, followed by ultracentrifugation of viral supernatant as described[62]. Generation of vesicular stomatitis virus (VSV, viral titer was 4 × 10^{11} unit/ml) for tracing neuronal connections in vivo was done as previously described[54]. Briefly, the rVSV-EGFP with the EGFP in the first genome position was amplified in baby hamster kidney BSR T7/5 cells (gift of S. P. Whelan) and purified as described previously[63]. At 100% confluency BSR T7/5 cells were infected with rVSV-EGFP at an MOI of 0.01 and the supernatant are collected 2 day later. The supernatant was concentrated by ultracentrifugation at 21,000 rpm in an SW28 rotor (Beckman Coulter) for 3 hours at 4°C. Virus pellets were resuspended overnight in phosphate buffered saline (PBS) with 25 mM HEPES. The virus resuspension was purified on linear 15-45% sucrose gradients prepared in the NTE buffer (10 mM Tris pH 7.4, 100 mM NaCl, 1 mM EDTA). The sucrose gradient was centrifuged at 25,000 rpm in an SW41 rotor (Beckman Coulter) for 5 hours at 4°C. The virus band was collected and then aliquoted and frozen in −80°C before use. The rVSV-EGFP virus was titrated with BSR T7/5 cells and DMEM-agarose (0.33%) overlay and the titre was 4 × 10^{11} unit/ml. The pAAVTRE-ChR2-eYFP construct was obtained from Dr. Sussumu Tonegawa (MIT)[25]. The recombinant AAV vectors were serotyped with AAV_9 coat proteins and packaged by Boston Children's Hospital Viral Core at the Harvard Medical School. Viral titer was 4.956 × 10^{14} genome copy/ml for AAV_9-TRE:ChR2-eYFP. AAV_9-TRE:ChR2-mCherry titre was 8 × 10^{12} unit/ml (a gift from Dr. Steve Ramirez). $rAAV_5$/

CamkII-hChr2(H134R)-eYFP virus was generated at the University of North Carolina at Chapel Hill (UNC) Vector Core and viral titer was 8.5×10^{12} genome copy/ml.

Stereotactic viral injection

Mice were anaesthetized with ketamine/xylazine (10 mg mL^{-1} and 1.6 mg mL^{-1}). Mice were placed in the stereotaxic apparatus and a small hole was drilled at each injection location. The needle was slowly lowered into the target site and remained for 5 min prior to injection. Virus was injected using a Hamilton microsyringe (0.1 μl/min) into the dorsal DG using the following coordinates: Adult (3-4 months old) and Aged (17-18 month old) mice, anterioposterior = −1.8 mm from bregma; lateral = ± 1.5 mm; depth = 2.5 mm; 4-5 weeks old juvenile mice, anterioposterior = −1.7 mm from bregma; lateral = ± 1.45 mm; depth = 2.4 mm). Injection needles were left in place for additional 10 min after injection to ensure even distribution of the virus and then slowly withdrawn. The skin incision was carefully sutured after viral injection to minimize inflammation. 0.5 μl Lentiviral-shNT, lentiviral-shRNA (unless otherwise specified, Lentiviral shRNA #46 injected through the study), or AAV_9-TRE-ChR2-eYFP was injected bilaterally into dorsal DG. 0.1μl diluted vesicular stomatitis virus (1:10 of original virus stock) was injected unilaterally into dorsal DG. Mice were given carprofen (5 mg kg^{-1}) prior to and during surgery, and 24 h later to minimize discomfort. All injection sites were verified histologically. Only mice with virus expression limited to the targeted regions were included for analysis.

Optical fiber implant

A viral cocktail (0.5 μl Lentiviral-shNT or lentiviral-shNT/RNA and 0.5 μl AAV_9-TRE-ChR2-eYFP or AAV_9-TRE-ChR2-mcherry) was injected bilaterally into dorsal DG of adult (3-4 months) cfos-tTA mice. 1 week after injections, optical fiber implant surgeries were performed to the same mice. 200 μm core, 0.37 numerical aperture (NA) multimode fiber (ThorLabs) was threaded through and glued with epoxy to a 230 μm core stainless steel or zirconia multimode ferrule (Fiber Instrument Sales and Precision Fiber Products), polished and cut for implantation. Optical patch cables were generated the same way with the free end connected to a multimode FC ferrule assembly for connecting to a 1×2 Optical rotary joint (Doric lenses). The other end of the rotary joint was connected via a patch cable to either a 100 mw 473 nm laser diode (OEM laser systems) via a non-contact style laser to fiber coupler (OZ optics). Mice were anaesthetized with ketamine/xylazine (10 mg mL^{-1} and 1.6 mg mL^{-1}), placed in the stereotaxic apparatus and the optical fiber was lowered into the injection site (–1.8 mm AP; ± 1.5 mm ML; −1.75 mm DV). The implant was secured to the skull with two jewelry screws, adhesive super glue (Loctite Adhesives) and dental cement. Mice were given carprofen (5 mg kg^{-1}) prior to, during and after surgery to minimize discomfort. Mice were allowed to recover for 2 weeks before behavioral experiments.

Whole-cell electrophysiological recordings

2 weeks after lentiviral-shNT/shRNA injection into 4-5 weeks old PV-cre:Ai14 mice, mice were used for slice electrophysiology. Briefly, 300 μm hippocampal sections were cut in an ice slush solution containing (in mM): 85 NaCl, 75 Sucrose, 2.5 KCl, 1.3 NaH2PO4, 24 NaHCO3, 0.5 CaCl2, 4 MgCl2, 25 D-Glucose. Slices were allowed to recovere for 30’ at

31.5°C in ACSF containing (in mM): 126 NaCl, 2.5 KCl, 1 NaH2PO4, 26.2 NaHCO3, 2.5 CaCl2, 1.3 MgSO4, 11 D-Glucose. Whole-cell recordings were made using an Axopatch 700B amplifier (Molecular Devices) with filtering at 1 KHz using 4-6 MΩ electrodes. For mEPSCs, electrodes were filled with an internal solution containing (in mM): 120 CsMeSO3, 5 MgCl2, 8 NaCl, 1 EGTA, 10 HEPES, 1 QX-314, 0.5 Na3GTP, 2 MgATP, pH 7.2-7.3, 280-290 mOsm. For mIPSCs, electrodes were filled with an internal solution containing (in mM): 140 CsCl, 0.2 CaCl2, 8 NaCl, 2 EGTA, 10 HEPES, 1 QX-314, 0.5 Na3GTP, 4 MgATP, pH 7.2-7.3, 280-290 mOsm. For analysis of light-evoked EPSCs and IPSCs in CA3, a viral cocktail including 0.5 μl lentiviral-shNT or lentiviral-shRNA and 0.3 μl $rAAV_5$-ChR2-eYFP (1:10 of original dilution) was injected unilaterally into dorsal DG of adult (3-4 months) B6 mice that were subsequently used for slice electrophysiology. Electrodes were filled with an internal solution containing (in mM): 132 CsMeSO3, 8 CsCl, 10 HEPES, 1 EGTA, 0.5 CaCl2, 10 Glucose, 1 QX-314, pH 7.2-7.3, 280-290 mOsm. Cutting and ACSF solutions were continually bubbled with O2/CO2, and all recordings were made in ACSF at 32°C continually perfused over slices at a rate of ~2 ml/min. mEPSC recordings were made in the presence of tetrodotoxin (500 nM) and picrotoxin (100 μM). mIPSC recordings were made in the presence of tetrodotoxin and kynurenic acid (2 mM). For mEPSC and mIPSC recordings, neurons were held in voltage clamp at −60 mV. Miniature events were analyzed using MiniAnalysis software (Synaptosoft) using automatic detection with visual confirmation of events. For light-evoked EPSCs, neurons were held at −70 mV, and for light-evoked IPSCs, neurons were held at 0 mV. Responses were elicited with a 5 ms blue light pulse delivered at 0.1 Hz via a fiber optic placed above the DG in slice. Peak current amplitudes were measured from an average of at least 10 traces.

Behavioral procedures

2 weeks after stereotactic viral injection or optical fiber implant, mice were subjected to behavioral experiments. For the cohorts of adult C57Bl/6 mice (3-4 months old) and aged C57Bl/6 mice (17-18 months old) with lentiviral-shNT/shRNA injection, behavioral tasks were performed in the following order: open field test (day 1), dark-light test and elevated plus maze test (day 2), tail suspension test (day 3). Contextual fear conditioning was performed 2 days after tail suspension test. For the cohorts of TetTag mice, mice were raised and maintained on doxycycline (dox) diet (40 mg kg^{-1} chow). 2 weeks after surgery, mice were habituated to transportation and external environmental cues by being carted out of the animal facility into the experimental rooms and handled for 5 minute in the experimental room each day for three days before the experiment. Following the third habituation session, mice were fed regular food without Dox for 3 days until contextual fear conditioning training. After the training trial, mice were returned to their home cage and placed on Dox chow to turn off reporter gene expression. For the cohorts used for the optogenetic engram stimulation experiment, a similar protocol was used as described above except that mice were taken off Dox for 2 days before contextual fear conditioning. Following behavioral testing, brain sections were examined to confirm efficient viral labeling in target areas. Animals with mistargeted viral labeling were excluded before behavior quantification.

Open field paradigm—Open field paradigm was performed as done previously[64]. Mice were kept in a quiet, holding area for at least 30 min before the test. Motor activity over 30

min was quantified in four Plexiglas open-field boxes of 41 × 41cm (Kinder Scientific) with 16 sets of double stacked pulse-modulated infrared photobeams equally spaced on every wall (128 total) to record x–y ambulatory movements. The software defined grid lines that divided each open field into center and surround regions with the periphery consisting of the 10cm closest to the wall around the entire perimeter. Dependent measures were the total distance traveled (in centimeters), time spent in the center (s) and rearing events through 30 min recording period.

Light-dark test—The light-dark test was conducted in the open-field chamber as described above but with a dark plastic box that is opaque to visible light but transparent to infrared covering one-half of the chamber area, thus creating dark and light compartments of equal size. An opening at floor level in the center of one wall of the dark compartment allowed passage between the light and dark compartments. The light compartment was brightly illuminated. Mice were kept in a quiet, holding area for at least 30 min before the test. Between each trial, the whole apparatus was cleaned. At the beginning of the test, the mouse was placed in the dark compartment and allowed to freely explore both compartments for 10 min. Ambulation distance and time spent in the dark and the light compartments were recorded.

Elevated Plus Maze test—Elevated Plus Maze test was performed as done previously[64]. The elevated plus maze consisted of black Plexiglass apparatus with four arms (16 cm long and 5 cm wide) set in a cross from a neutral central square (5 cm × 5 cm) placed 1m above the floor. Two opposing arms were delimited by vertical walls (closed arms), while the two other opposing arms had unprotected edges (open arms). Mice were placed in the center and their behavior was recorded for 5 min via a video camera system (ViewPoint, Lyon, France) located above the maze. Cumulative time spent in the open and closed arms were scored manually by investigators blind to the treatment conditions. An arm visit was recorded when the mouse placed both its forepaws in the arm.

Tail suspension test—Mice were suspended 50 cm above a solid surface by the use of adhesive tape applied to the tail. A “cushioned” surface with mouse bedding below the TST was placed to help prevent injury to the falling animal. The animal’s behavior was recorded for 6 min using an automated video-tracking system. Struggling and climbing behaviors were analyzed using View-Point Life Sciences software.

Contextual fear conditioning—Conditioning was conducted in Coulbourn Habitest fear conditioning chambers as done previously[64]. With clear front and back Plexiglas walls, aluminum side walls, and stainless-steel bars as a floor. The chamber was lit from above with a light, ventilated with a fan, and encased by a sound-dampening cubicle. On the days of training and testing, mice were brought out of the animal facility and allowed to habituate for 1 h outside the testing room before starting the experiment. Mouse behavior was recorded by digital video cameras mounted above the conditioning chamber. For the training context (designated A throughout), the fan and lights were left on, stainless-steel bars were exposed, and ethanol was used as an olfactory cue. Mice were brought into the behavioral room in a standard housing cage. For neutral context (designated C throughout), mice were

brought into the behavioral room in cardboard buckets. Mice were placed in individual round white cardboard paper chamber inside a large plastic container. On the training day, mice were kept in a quiet, holding area for at least 1 h before the training. During training, mice were placed for 180 s in the conditioning chamber and received three shocks (2 s, 0.75 mA) at 180 s, 240 s, 300 s. Mice were taken out 60 s after termination of the third footshock and kept in a quiet area for additional 30 min before being returned to animal facility. For acquisition, freezing levels were quantified over the initial 180s prior to the shock (baseline) and 60 s after each footshock. Freezeframe and Freezeview software (Actimetrics) were used for recording and analyzing freezing behavior, respectively.

For the multiple exposure paradigm (day 1, 10 and 16 after training), animals were exposed to the training context (context A) and a neutral context (context C) for 3 min in a counterbalanced design with the second exposure 2 h following the initial test. Freezing levels were quantified over the 3 min exposure period. For limited exposure paradigm, animals were exposed to the training context (context A) for 3 min on day 1. Then the same animals were exposed to the training context (context A) and a neutral context (context C) for 3 min in a counterbalanced design at day 16. Freezing levels were quantified over the 3 min exposure period. Mice were perfused 1 h after context exposure to examine neuronal activation. cfos-tTA:teto-TauLacZ mice were perfused 24 h or 16 days after contextual fear conditioning and indelible labeling to examine engram connectivity. cfostTA:teto-h2B-GFP and cfostTA:teto-h2B-mcherry mice were exposed to the training context (context A) or a neutral context (context C) for 3 min at day 1 or day 16 after contextual fear conditioning. Mice were perfused 1 h after context exposure to examine neuronal ensemble reactivation at different time points.

For the optical stimulation experiments, mice were allowed to explore context C for 6 min 2 days and 10 days after contextual fear conditioning training. Prior to each test session, fibre implants were attached to the patch cables via a zirconia sleeve and mice were left for 30-60 s in a transition cage similar to their home cage. The patch cables were interfaced to an FC/PC rotary joint (Doric lenses) that was attached on the other end to a laser diode. The 6 min session was divided into two 3-min epochs, the first a light-off epoch and the second a light-on epoch. During the light-on epochs, mice received blue light stimulation (473 nm, 9 mW, 20 Hz, 15 ms) for 3 min duration. At the end of 6 min the mouse was immediately detached from the laser and returned to its home cage. The no shock (NS) group went through the same habituation, training and test sessions as the experimental group except that no foot shocks were given during the training session. Light stimulation during test sessions interfered with motion detection of the program and therefore, experimenters manually scored the freezing behavior while blind to identity of group.

In situ hybridization

In situ hybridization (ISH) was performed using dioxygenin-labeled riboprobes on 35 μm cryosections generated from perfused tissue as described previously[64]. Premixed RNA labeling nucleotide mixes containing digoxigenin-labeled UTP (Roche Molecular Biochemicals) were used to generate RNA riboprobes. *Ablim3* antisense probe sequence was obtained from Allen Brain Atlas (Probe RP_051214_03_D07, http://mouse.brain-

map.org/experiment/show?id=73992943). Sense probe was generated as a negative control. Riboprobes were purified on G-50 Microspin columns (GE Healthcare). Probe concentration was confirmed by Nanodrop prior to the addition of formamide. Briefly, sections were mounted on charged glass (Superfrost Plus) slides and postfixed for in 4% paraformaldehyde (PFA). Sections were then washed in DEPC-treated PBS, treated with proteinase K (40 μg/ml final), washed again in DEPC-treated PBS, and then acetylated. Following prehybridization, sections were incubated with riboprobe overnight at 58°, washed in decreasing concentrations of SSC buffer, and immunological detection was carried out with anti-Dioxygenin antibody conjugated with alkaline phosphatase (Roche). Color reaction was carried out with NBT/BCIP. Color reaction times were identical for both treatment groups. Images were acquired with an epifluorescence microscope (Nikon) using a 10× objective. For quantification, 2-4 color images per region per mouse were analyzed using the mean intensity function in Image J. All images were captured using the same light intensity and exposure times. The mean intensity of the region of interest (minus mean intensity of a selected background region) was averaged across images for each mouse and each treatment group.

Immunohistochemistry

35 μm cryosections obtained from perfused tissue were stored in PBS with 0.01% sodium azide at 4°C. For immunostaining, floating sections were washed in PBS, blocked (in PBS containing 0.3% Triton X-100 and 10% NDS) and incubated with primary antibody overnight at 4 °C overnight (rabbit anti c-fos, Calbiochem PC38, 1:10,000 – discontinued; different batches of rabbit, Santa Cruz SC52, 1:2,000; rabbit anti-GFP, Life Technologies A11122, 1:500; Guinea-pig anti-GABA, Millipore AB175, 1:500; mouse anti-PV, Millipore MAB1572, 1:2,000; mouse anti-SST, Santa Cruz, sc-55565, 1:100; mouse anti-RGS14, Biolegend N133/21, 1:400; chicken anti-β-galactosidease, Abcam, 1:1000; Guinea pig anti-VGLUT1, Synaptic Systems 135304, 1:3000; Mouse anti-NeuN, Millipore MAB377; Goat anti- Doublecortin (DCX) sc-8066, Santa Cruz, 1:500). On day 2, sections were rinsed three times for 10 min in PBS and incubated for 90 min with Fluorescent-label-coupled secondary antibody (Jackson ImmunoResearch, 1:500). Sections were rinsed three times for 10 min each in PBS before mounting on to glass slides and coverslipped with mounting media containing DAPI (Fluoromount with DAPI, Southern Biotech). abLIM3 immunostaining was performed as described previously[52]. Briefly, to analyze the distribution of abLIM3 in hippocampus, fresh frozen sections were mounted on glass slides, air-dried and sequentially fixed in 95% ethanol at −20 °C for 30 min and 100% acetone at room temperature for 1 min. The slides were blocked with 1% BSA in PBS for 30 min, and incubated with primary antibodies at room temperature for 2 h (mouse anti-abLIM3, Abcam ab67721, 1:100; Guinea pig anti-VGLUT1, Synaptic Systems 135304, 1:3000; rabbit anti-bassoon, Abcam ab110426, 1:1000; rabbit anti-ZO-1 antibody, Invitrogen 402200, 1:500). After washing with PBS, the slides were incubated with fluorescence-conjugated secondary antibodies (Jackson ImmunoResearch, 1:500), for 30 min and then coverslipped with mounting media containing DAPI (Fluoromount with DAPI, Southern Biotech).

Images acquisition and analysis

Images were obtained from one set of brain sections (6 sets generated for each brain) for each immunostaining experiment (set of antigens). All analysis was performed by an experimenter blind to group identity.

Image analysis of mossy fiber terminals—A Nikon A1R Si confocal laser, a TiE inverted research microscope, and NIS Elements software were used to capture z-stacks for Mossy fiber terminal (MFT) imaging using a 60 × objective plus 10 × digital zoom.as we previously published[65]. Mossy fiber axons of dentate granule cells were imaged in stratum lucidum of CA3ab. Images were obtained from high-resolution (2048 resolution) image Z-stacks with a step size of 0.3 μm. Area of individual MFTs was assessed at the widest point in the Z-stack using Image J image>stacks>Z projection, followed by unbiased area selection with the tracing tool. MFTs were defined as having a cross sectional area of 4 μm^2 or greater[28] from lentiviral-shNT/shRNA injected samples. MFT Filopodia extensions were also quantified. MFT Filopodia extensions were defined as protrusions exceeding 1 μm in length and possessing an end-swelling varicosity structure. At least 20-30 MFTs from each animal were imaged for MFT and MFT filopodia measurements.

Image analysis of dendritic spines—For quantification of dendritic spines, confocal z-stack images were acquired using a Nikon A1R Si confocal laser, a TiE inverted research microscope, and NIS Elements software. Imaging was performed using a 60 × objective, plus and 6× digital zoom. For spine imaging, confocal z-stacks (2048 resolution) with 0.3 μm step size were taken centered on dendritic segment. Z-stacks were flattened using the maximum intensity projection, and flattened images were quantified using image J. For spine density, spines were counted manually for at least 100 μm of dendritic length per region per mouse. The outer molecular layer was defined as the outer 1/3 of the molecular layer of DG.

To quantify cfos+ cells and overlap in antigens (GFP/GABA, GFP/PV, c-Fos/PV, c-Fos/SST, cfos/H2B-mCherry, H2B-GFP/cfos, TdTomato/PV, DCX/GFP), z-stack images were acquired with a Nikon A1R Si confocal laser, a TiE inverted research microscope using a 20 × objective. Images (1024 resolution) were acquired as 11 μm z-stacks with a step size of 1 μm. For quantification of c-Fos+ cells in the region of interest (ROI), maximum intensity projection image was generated from 11 z-stack images with ImageJ, and the cell signal intensity above background within the same image was computed. For overlapping quantification, double positive cells were annotated in maximum intensity projection image by multi-point tool and carefully examined within each z-stack image to confirm co-localization and confirmed using the DAPI staining.

For overlap by chance quantification, fifty DAPI+ cells were randomly selected within the manually defined region of interest (ROI) on each image used for quantification of reactivation. Because of the high cell density in the DG, seventy-five DAPI+ cells were randomly selected for chance-overlap quantification in the DG. The number of cFos+ and GFP+ cells among the randomly selected cells were then determined by examination of overlap in the appropriate channels for each Tet-Tag system. Chance overlap was defined as

the product of the probability of a randomly selected cell being cFos+ and the probability of such a cell being GFP+ (%cFos+ * %GFP+). A minimum of four regions in different hemisections were analyzed per animal to calculate an “average chance overlap” per animal.

To quantify PV puncta density in CA3, images were acquired with a Nikon A1R Si confocal laser, a TiE inverted research microscope using a 60 × objective plus 4 × digital zoom. Puncta number was counted in each image and the area per image was measured with ImageJ. Image size was constant for each section (2812.5 μm^2) and among all animals. Puncta density was defined as the number of puncta per 1000 μm^2. For each animal, puncta density was averaged from 3 images of CA3ab region.

Statistical Analysis

Statistical analysis was carried out using GraphPad Prism software. Comparison of two groups was performed using two-tailed student’s unpaired t-test unless otherwise specified. Comparison of one group across time was performed using a one-way ANOVA with repeated measure. Comparison of two groups across treatment condition or time was performed using a two-way repeated measure ANOVA and main effects or interactions were followed by Bonferroni post-hoc analysis. mEPSCs and mIPSCs were analyzed using Komolgrov-Smirnov tests with significance set at $P < 0.0001$. In the text and figure legends, “n” indicates number of mice per group. Detailed statistical analyses can be found in Supplementary table 1 and Life Sciences Reporting Summary.

Supplementary Material

Refer to Web version on PubMed Central for supplementary material.

Acknowledgments

We wish to thank members of the Sahay lab for comments on the manuscript and the late N.J. Sahay for advice. We are thankful to S. Tonegawa for providing us with AAV9 tetO ChR2 construct, M. Greenberg for Lentiviral pLLX vector, S. Ramirez for providing us with AAV9- tetO ChR2-mCherry virus. L.Z is supported by R01MH104450. C.C is an investigator of the Howard Hughes Medical Institute. A.S acknowledges support from US National Institutes of Health Biobehavioral Research Awards for Innovative New Scientists (BRAINS) R01MH104175, NIH-NIA R01AG048908, NIH 1R01MH111729, Ellison Medical Foundation New Scholar in Aging, Whitehall Foundation, Inscopix Decode award, NARSAD Independent Investigator Award, Ellison Family Philanthropic support, Blue Guitar Fund, Harvard Neurodiscovery Center/MADRC Center Pilot Grant Award, Harvard Stem Cell Institute Development grant and HSCI seed grant. C.H was supported by 2016 HSCI Harvard Internship Program Award.

References

1. Jasnow AM, Lynch JF 3rd, Gilman TL, Riccio DC. Perspectives on fear generalization and its implications for emotional disorders. Journal of neuroscience research. 2017; 95:821–835. DOI: 10.1002/jnr.23837 [PubMed: 27448175]
2. Biedenkapp, JC., Rudy, JW. Learning & memory. Vol. 14. Cold Spring Harbor; N.Y: 2007. Context preexposure prevents forgetting of a contextual fear memory: implication for regional changes in brain activation patterns associated with recent and remote memory tests; p. 200-203.
3. Wiltgen, BJ., Silva, AJ. Learning & memory. Vol. 14. Cold Spring Harbor; N.Y: 2007. Memory for context becomes less specific with time; p. 313-317.
4. Poulos, AM., et al. Learning & memory. Vol. 23. Cold Spring Harbor; N.Y: 2016. Conditioning- and time-dependent increases in context fear and generalization; p. 379-385.

5. Besnard A, Sahay A. Adult Hippocampal Neurogenesis, Fear Generalization, and Stress. Neuropsychopharmacology. 2016; 41:24–44. DOI: 10.1038/npp.2015.167 [PubMed: 26068726]
6. Liberzon I, Abelson JL. Context Processing the Neurobiology of Post-Traumatic Stress Disorder. Neuron. 2016; 92:14–30. DOI: 10.1016/j.neuron.2016.09.039 [PubMed: 27710783]
7. Jovanovic T, Ressler KJ. How the neurocircuitry and genetics of fear inhibition may inform our understanding of PTSD. Am J Psychiatry. 2010; 167:648–662. DOI: 10.1176/appi.ajp.2009.09071074 [PubMed: 20231322]
8. Leal SL, Yassa MA. Neurocognitive Aging the Hippocampus across Species. Trends Neurosci. 2015; 38:800–812. DOI: 10.1016/j.tins.2015.10.003 [PubMed: 26607684]
9. Bakker A, et al. Reduction of hippocampal hyperactivity improves cognition in amnestic mild cognitive impairment. Neuron. 2012; 74:467–474. DOI: 10.1016/j.neuron.2012.03.023 [PubMed: 22578498]
10. Xu W, Sudhof TC. A neural circuit for memory specificity and generalization. Science. 2013; 339:1290–1295. DOI: 10.1126/science.1229534 [PubMed: 23493706]
11. Ruediger S, et al. Learning-related feedforward inhibitory connectivity growth required for memory precision. Nature. 2011; 473:514–518. DOI: 10.1038/nature09946 [PubMed: 21532590]
12. Kheirbek MA, Klemenhagen KC, Sahay A, Hen R. Neurogenesis and generalization: a new approach to stratify and treat anxiety disorders. Nat Neurosci. 2012; 15:1613–1620. DOI: 10.1038/nn.3262 [PubMed: 23187693]
13. Likhtik E, Stujenske JM, Topiwala MA, Harris AZ, Gordon JA. Prefrontal entrainment of amygdala activity signals safety in learned fear and innate anxiety. Nat Neurosci. 2014; 17:106–113. DOI: 10.1038/nn.3582 [PubMed: 24241397]
14. Jones GL, et al. A genetic link between discriminative fear coding by the lateral amygdala, dopamine, and fear generalization. eLife. 2015; 4
15. Lynch JF, Winiecki P, Gilman TL, Adkins JM, Jasnow AM. Hippocampal GABAB (1a) Receptors Constrain Generalized Contextual Fear. Neuropsychopharmacology. 2017; 42:914–924. DOI: 10.1038/npp.2016.255 [PubMed: 27834391]
16. McClelland JL, McNaughton BL, O'Reilly RC. Why there are complementary learning systems in the hippocampus and neocortex: insights from the successes and failures of connectionist models of learning and memory. Psychological review. 1995; 102:419–457. [PubMed: 7624455]
17. Frankland PW, Bontempi B. The organization of recent and remote memories. Nature reviews Neuroscience. 2005; 6:119–130. DOI: 10.1038/nrn1607 [PubMed: 15685217]
18. Winocur G, Moscovitch M, Sekeres M. Memory consolidation or transformation: context manipulation and hippocampal representations of memory. Nat Neurosci. 2007; 10:555–557. DOI: 10.1038/nn1880 [PubMed: 17396121]
19. Wiltgen BJ, et al. The hippocampus plays a selective role in the retrieval of detailed contextual memories. Curr Biol. 2010; 20:1336–1344. DOI: 10.1016/j.cub.2010.06.068 [PubMed: 20637623]
20. Winocur G, Moscovitch M, Bontempi B. Memory formation and long-term retention in humans and animals: convergence towards a transformation account of hippocampal-neocortical interactions. Neuropsychologia. 2010; 48:2339–2356. DOI: 10.1016/j.neuropsychologia.2010.04.016 [PubMed: 20430044]
21. Teyler TJ, Rudy JW. The hippocampal indexing theory and episodic memory: updating the index. Hippocampus. 2007; 17:1158–1169. DOI: 10.1002/hipo.20350 [PubMed: 17696170]
22. Hardt O, Nader K, Nadel L. Decay happens: the role of active forgetting in memory. Trends in cognitive sciences. 2013; 17:111–120. DOI: 10.1016/j.tics.2013.01.001 [PubMed: 23369831]
23. Frankland PW, Bontempi B, Talton LE, Kaczmarek L, Silva AJ. The involvement of the anterior cingulate cortex in remote contextual fear memory. Science. 2004; 304:881–883. DOI: 10.1126/science.1094804 [PubMed: 15131309]
24. Liu X, Ramirez S, Redondo RL, Tonegawa S. Identification and Manipulation of Memory Engram Cells. Cold Spring Harb Symp Quant Biol. 2015
25. Kitamura T, et al. Engrams and circuits crucial for systems consolidation of a memory. Science. 2017; 356:73–78. DOI: 10.1126/science.aam6808 [PubMed: 28386011]

26. Acsady L, Kamondi A, Sik A, Freund T, Buzsaki G. GABAergic cells are the major postsynaptic targets of mossy fibers in the rat hippocampus. J Neurosci. 1998; 18:3386–3403. [PubMed: 9547246]
27. Martin EA, et al. The intellectual disability gene Kirrel3 regulates target-specific mossy fiber synapse development in the hippocampus. eLife. 2015; 4:e09395. [PubMed: 26575286]
28. Torborg CL, Nakashiba T, Tonegawa S, McBain CJ. Control of CA3 output by feedforward inhibition despite developmental changes in the excitation-inhibition balance. The Journal of neuroscience: the official journal of the Society for Neuroscience. 2010; 30:15628–15637. DOI: 10.1523/JNEUROSCI.3099-10.2010 [PubMed: 21084618]
29. Mori M, Abegg MH, Gahwiler BH, Gerber U. A frequency-dependent switch from inhibition to excitation in a hippocampal unitary circuit. Nature. 2004; 431:453–456. DOI: 10.1038/nature02854 [PubMed: 15386013]
30. Porro F, et al. beta-adducin (Add2) KO mice show synaptic plasticity, motor coordination and behavioral deficits accompanied by changes in the expression and phosphorylation levels of the alpha- and gamma-adducin subunits. Genes Brain Behav. 2010; 9:84–96. DOI: 10.1111/j.1601-183X.2009.00537.x [PubMed: 19900187]
31. Rabenstein RL, et al. Impaired synaptic plasticity and learning in mice lacking beta-adducin, an actin-regulating protein. J Neurosci. 2005; 25:2138–2145. DOI: 10.1523/JNEUROSCI.3530-04.2005 [PubMed: 15728854]
32. Buzsaki G. Hippocampal sharp wave-ripple: A cognitive biomarker for episodic memory and planning. Hippocampus. 2015; 25:1073–1188. DOI: 10.1002/hipo.22488 [PubMed: 26135716]
33. Gan J, Weng SM, Pernia-Andrade AJ, Csicsvari J, Jonas P. Phase-Locked Inhibition, but Not Excitation, Underlies Hippocampal Ripple Oscillations in Awake Mice In Vivo. Neuron. 2016
34. Jadhav SP, Kemere C, German PW, Frank LM. Awake hippocampal sharp-wave ripples support spatial memory. Science. 2012; 336:1454–1458. DOI: 10.1126/science.1217230 [PubMed: 22555434]
35. Ognjanovski N, et al. Parvalbumin-expressing interneurons coordinate hippocampal network dynamics required for memory consolidation. Nature communications. 2017; 8:15039.
36. Nakashiba T, Buhl DL, McHugh TJ, Tonegawa S. Hippocampal CA3 output is crucial for ripple-associated reactivation and consolidation of memory. Neuron. 2009; 62:781–787. DOI: 10.1016/j.neuron.2009.05.013 [PubMed: 19555647]
37. Caliskan G, et al. Identification of Parvalbumin Interneurons as Cellular Substrate of Fear Memory Persistence. Cereb Cortex. 2016; 26:2325–2340. DOI: 10.1093/cercor/bhw001 [PubMed: 26908632]
38. Wilson IA, Ikonen S, Gallagher M, Eichenbaum H, Tanila H. Age-associated alterations of hippocampal place cells are subregion specific. J Neurosci. 2005; 25:6877–6886. DOI: 10.1523/JNEUROSCI.1744-05.2005 [PubMed: 16033897]
39. Yassa MA, et al. Pattern separation deficits associated with increased hippocampal CA3 and dentate gyrus activity in nondemented older adults. Hippocampus. 2011; 21:968–979. DOI: 10.1002/hipo.20808 [PubMed: 20865732]
40. Simkin D, et al. Aging-Related Hyperexcitability in CA3 Pyramidal Neurons Is Mediated by Enhanced A-Type K+ Channel Function and Expression. J Neurosci. 2015; 35:13206–13218. DOI: 10.1523/JNEUROSCI.0193-15.2015 [PubMed: 26400949]
41. Thome A, Gray DT, Erickson CA, Lipa P, Barnes CA. Memory impairment in aged primates is associated with region-specific network dysfunction. Mol Psychiatry. 2016; 21:1257–1262. DOI: 10.1038/mp.2015.160 [PubMed: 26503764]
42. Villanueva-Castillo C, Tecuatl C, Herrera-Lopez G, Galvan EJ. Aging-related impairments of hippocampal mossy fibers synapses on CA3 pyramidal cells. Neurobiol Aging. 2017; 49:119–137. DOI: 10.1016/j.neurobiolaging.2016.09.010 [PubMed: 27794263]
43. Geinisman Y, de Toledo-Morrell L, Morrell F, Persina IS, Rossi M. Age-related loss of axospinous synapses formed by two afferent systems in the rat dentate gyrus as revealed by the unbiased stereological dissector technique. Hippocampus. 1992; 2:437–444. [PubMed: 1308200]

44. Reijmers LG, Perkins BL, Matsuo N, Mayford M. Localization of a stable neural correlate of associative memory. Science. 2007; 317:1230–1233. DOI: 10.1126/science.1143839 [PubMed: 17761885]

45. Scobie KN, et al. Kruppel-like factor 9 is necessary for late-phase neuronal maturation in the developing dentate gyrus and during adult hippocampal neurogenesis. J Neurosci. 2009; 29:9875–9887. DOI: 10.1523/JNEUROSCI.2260-09.2009 [PubMed: 19657039]

46. Lundquist EA, Herman RK, Shaw JE, Bargmann CI. UNC-115, a conserved protein with predicted LIM and actin-binding domains, mediates axon guidance in C. elegans. Neuron. 1998; 21:385–392. [PubMed: 9728919]

47. Barrientos T, et al. Two novel members of the ABLIM protein family, ABLIM-2 and -3, associate with STARS and directly bind F-actin. J Biol Chem. 2007; 282:8393–8403. DOI: 10.1074/jbc.M607549200 [PubMed: 17194709]

48. Matsuda M, Yamashita JK, Tsukita S, Furuse M. abLIM3 is a novel component of adherens junctions with actin-binding activity. European journal of cell biology. 2010; 89:807–816. DOI: 10.1016/j.ejcb.2010.07.009 [PubMed: 20709423]

49. Cao J, et al. miR-129-3p controls cilia assembly by regulating CP110 and actin dynamics. Nature cell biology. 2012; 14:697–706. DOI: 10.1038/ncb2512 [PubMed: 22684256]

50. Beier KT, et al. Anterograde or retrograde transsynaptic labeling of CNS neurons with vesicular stomatitis virus vectors. Proc Natl Acad Sci U S A. 2011; 108:15414–15419. DOI: 10.1073/pnas.1110854108 [PubMed: 21825165]

51. Kamiya H, Shinozaki H, Yamamoto C. Activation of metabotropic glutamate receptor type 2/3 suppresses transmission at rat hippocampal mossy fibre synapses. The Journal of physiology. 1996; 493(Pt 2):447–455. [PubMed: 8782108]

52. Liu X, et al. Optogenetic stimulation of a hippocampal engram activates fear memory recall. Nature. 2012; 484:381–385. DOI: 10.1038/nature11028 [PubMed: 22441246]

53. Goshen I, et al. Dynamics of retrieval strategies for remote memories. Cell. 2011; 147:678–689. DOI: 10.1016/j.cell.2011.09.033 [PubMed: 22019004]

54. Vazdarjanova A, McGaugh JL. Basolateral amygdala is involved in modulating consolidation of memory for classical fear conditioning. J Neurosci. 1999; 19:6615–6622. [PubMed: 10414989]

55. Redondo RL, et al. Bidirectional switch of the valence associated with a hippocampal contextual memory engram. Nature. 2014; 513:426–430. DOI: 10.1038/nature13725 [PubMed: 25162525]

56. Girardeau G, Inema I, Buzsaki G. Reactivations of emotional memory in the hippocampus-amygdala system during sleep. Nat Neurosci. 2017; 20:1634–1642. DOI: 10.1038/nn.4637 [PubMed: 28892057]

57. Yang C, Svitkina T. Filopodia initiation: focus on the Arp2/3 complex and formins. Cell Adh Migr. 2011; 5:402–408. DOI: 10.4161/cam.5.5.16971 [PubMed: 21975549]

58. Mejillano MR, et al. Lamellipodial versus filopodial mode of the actin nanomachinery: pivotal role of the filament barbed end. Cell. 2004; 118:363–373. DOI: 10.1016/j.cell.2004.07.019 [PubMed: 15294161]

59. Wilson MA, McNaughton BL. Reactivation of hippocampal ensemble memories during sleep. Science. 1994; 265:676–679. [PubMed: 8036517]

60. Bartos M, Alle H, Vida I. Role of microcircuit structure and input integration in hippocampal interneuron recruitment and plasticity. Neuropharmacology. 2011; 60:730–739. DOI: 10.1016/j.neuropharm.2010.12.017 [PubMed: 21195097]

Supplementary References

61. Zhou Z, et al. Brain-specific phosphorylation of MeCP2 regulates activity-dependent Bdnf transcription, dendritic growth, and spine maturation. Neuron. 2006; 52:255–269. DOI: 10.1016/j.neuron.2006.09.037 [PubMed: 17046689]

62. Lois C, Hong EJ, Pease S, Brown EJ, Baltimore D. Germline transmission and tissue-specific expression of transgenes delivered by lentiviral vectors. Science. 2002; 295:868–872. DOI: 10.1126/science.1067081 [PubMed: 11786607]

63. Drokhlyansky E, et al. The brain parenchyma has a type I interferon response that can limit virus spread. Proc Natl Acad Sci U S A. 2017; 114:E95–E104. DOI: 10.1073/pnas.1618157114 [PubMed: 27980033]

64. McAvoy KM, et al. Modulating Neuronal Competition Dynamics in the Dentate Gyrus to Rejuvenate Aging Memory Circuits. Neuron. 2016; 91:1356–1373. DOI: 10.1016/j.neuron.2016.08.009 [PubMed: 27593178]

65. Ikrar T, et al. Adult neurogenesis modifies excitability of the dentate gyrus. Frontiers in neural circuits. 2013; 7:204. [PubMed: 24421758]

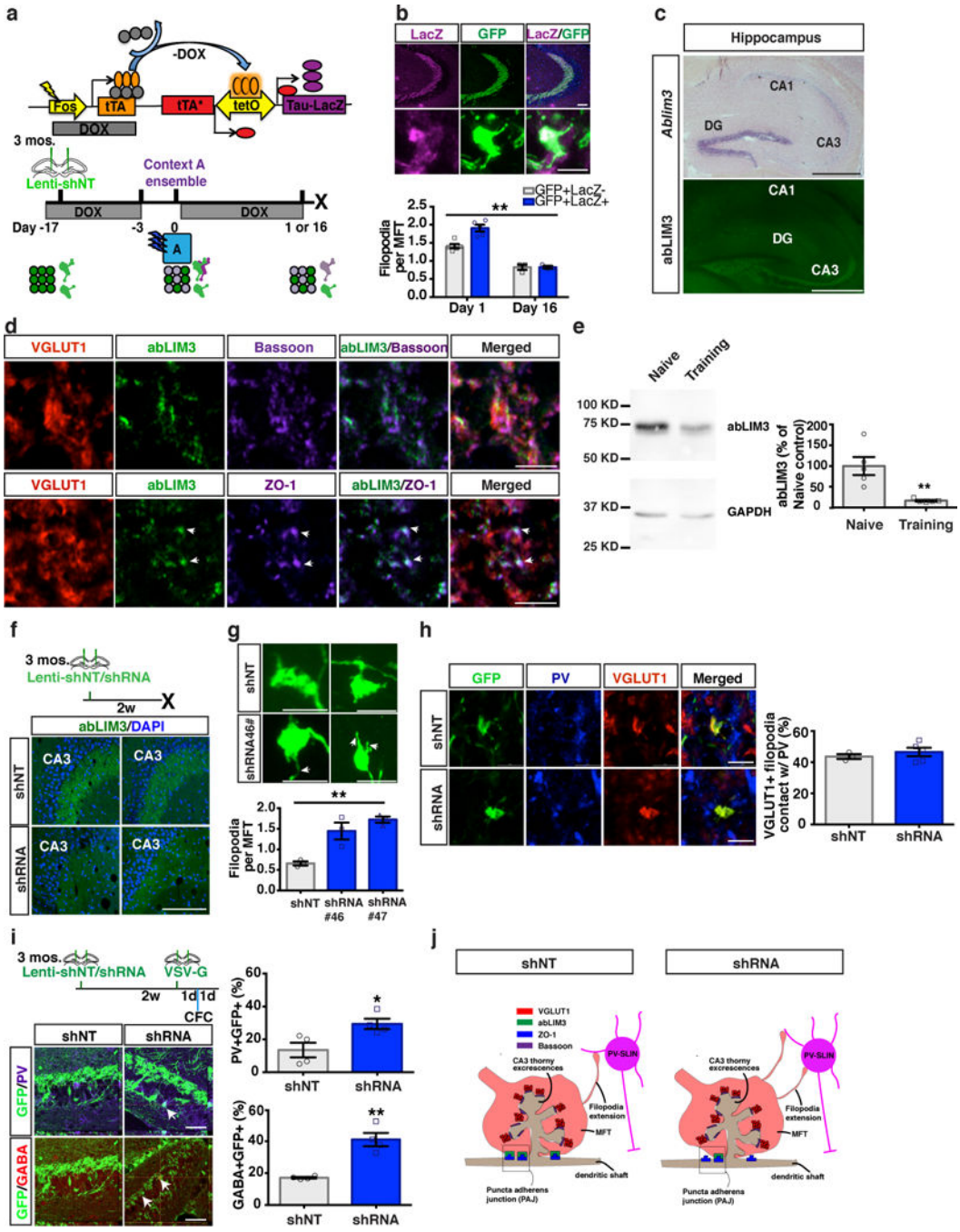

Figure 1. abLIM3 is a learning-regulated molecular brake of DGC-SLIN connectivity

(a) Schematic of Tet-off genetic system and behavioral schedule for labeling context A ensemble+ MFTs. (b) Images showing mossy fiber projections in hippocampus (*upper*) and an ensemble+ MFT (*lower*). Bar graph showing ensemble+ MFT filopodia (GFP+LacZ+) and non-ensemble/non-tagged MFTs (GFP+LacZ-) at day 1 and day 16 (89, 157 MFTs from day 1, 97, 115 MFTs from day 16. Two-way ANOVA, day X ensemble/non-ensemble MFT filopodia, F (1, 12) = 9.766, p=0.0088, Bonferroni post hoc: Day 1, p=0.0005; Day 16, p>0.9, n=5, 3 mice for each time point. (c) *In situ* hybridization showing *Ablim3* expression

in the hippocampus (*upper*), and abLIM3 immunohistochemistry (*Lower*). This experiment was replicated 3 times. (d) Triple immunofluorescence for abLIM3, ZO-1 (*lower*, arrows) and Bassoon (*upper*) in VGLUT1+ MFTs in CA3. This experiment was replicated 3 times. (e) Western blot analysis of abLIM3 levels in hippocampal lysates following learning (n=5,5 mice). The blot image (*left*) was cropped from supplementary Fig. 11d. Bar graph (*right*) was generated from full blot images in supplementary Fig. 11c. (f) Schematic of stereotaxic lentiviral injection into DG (*upper*) and representative images of abLIM3 immunohistochemistry in MFTs from 2 mice (shRNA#46 and shNT). This experiment was replicated 2 times. (g) Representative images showing GFP+ MFTs and filopodial extensions (arrows) following lentiviral shNT/shRNA-GFP injection (*upper*). Quantification of MFT-filopodia number (*lower*) (One-way ANOVA, p=0.0028, 77, 77 and 76 MFTs from n=3 mice in each group). (h) Images showing VGLUT1+ MFT and MFT filopodia contacting PV SLINs (*left*) and bar graphs with quantification of percentage of VGLUT1+ filopodia contacting PV (*right*) (85 filopodial extensions from 43 MFTs in shNT group, 115 filopodial extensions from 62 MFTs in shRNA group, n=3,5 mice). (i) Timeline of lentiviral-shNT/shRNA and VSV-G injection into DG (*left*). Contextual fear conditioning (CFC) was conducted 1d after VSV-G injection (*left, upper*). Confocal images showing anterograde labeled PV or GABA+ INs in CA3 (arrows) (*left, lower*) and bar graphs with quantification of percentage of GABA+GFP+ or PV+GFP+ cells in CA3 (n=4, 4 mice) (*right*). (j) Schematic showing distribution of abLIM3, Bassoon and ZO-1 in VGLUT1+ MFT and localization of abLIM3 to PAJs in lentiviral-shNT infected mice (*left*). Lentiviral shRNA mediated abLIM3 downregulation in MFTs induces generation of VGLUT1+ MFT filopodial contacts with PV SLINs (*right*). Scale bar represents 500 μm in c, 100 μm in b, f and h, 50 μm in i, and 5 μm in b, d, g and h. Unless otherwise specified, statistical comparisons were performed using two tailed unpaired t tests. **p < 0.01, *p < 0.05. Data are represented mean ± SEM. See supplementary Table 1.

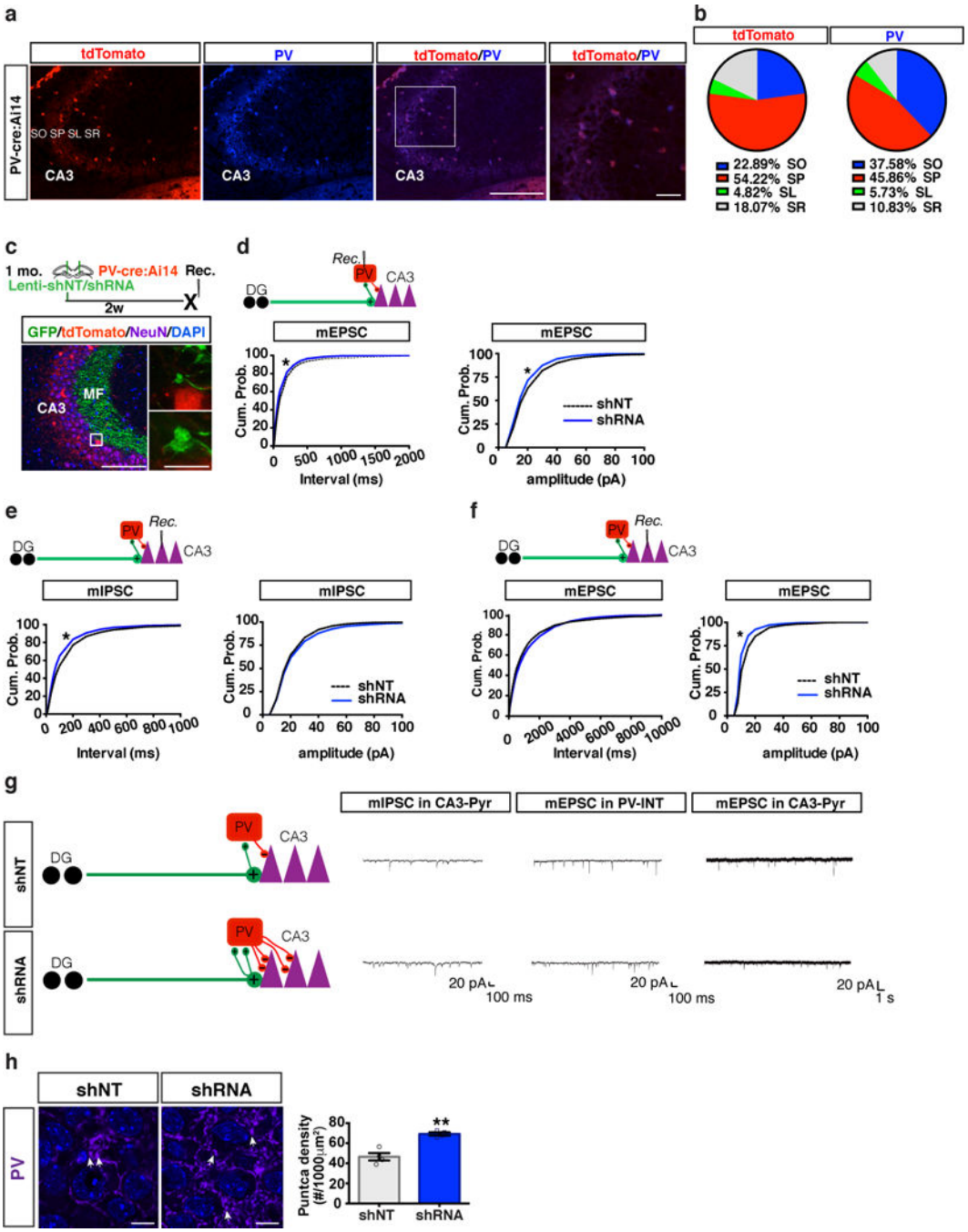

Figure 2. abLIM3 downregulation in DGCs increases mEPSCs in PV SLINs and PV puncta in CA3

(a) Representative images of genetically recombined tdTomato+ cells and PV+ cell (PV antibody staining) in CA3 of PV-Cre:Ai14 mice. Box highlights magnified regions (*left*). Immunostaining was replicated 2 times. (b) Pie graphs showing distribution of tdTomato + and PV+ cells in CA3 area including Stratum Pyramidale (SP), Stratum Oriens (SO) Stratum Radiatum (SR) and Stratum Lucidum (SL). (c) Schematic of lentiviral-shNT/shRNA injections into DG of PV- Cre:Ai14 mice (*upper*). Images showing lentiviral-shNT/shRNA infected GFP+ MFTs in PV- Cre:Ai14 mice, box highlights magnified regions (*lower*). (d)

Whole cell recording of mEPSC frequency (*left*, k-s test, $p < 0.0001$; shNT: 3887 events from n=13 cells, shRNA: 3588 events from n=12 cells, 3 mice per group) and mEPSC amplitude (*right*, k-s test, $p < 0.0001$; shNT: 3900 events from n=13 cells, shRNA: 3600 events from n=12 cells, 3 mice per group) from PV SLINs. (e) Intracellular recording of mIPSC frequency (*left*, k-s test, $p < 0.0001$; shNT: 2691 events from n=9 cells, shRNA: 2691 events from n=9 cells, 3 mice per group) and mIPSC amplitude (*right*, k-s test, $p = 0.0126$; shNT: 2700 events from n=9 cells, shRNA: 2700 events from n=9 cells, 3 mice per group) from CA3 Pyramidal neurons. (f) Intracellular recording of mEPSC frequency (*left*, k-s test, $p = 0.0222$ *middle*, k-s test, $p < 0.0001$; shNT: 1209 events from n=9 cells, shRNA: 1620 events from n=12 cells, 3 mice per group) and mEPSC amplitude (*right*, k-s test, $p < 0.0001$; shNT: 1218 events from n=9 cells, shRNA: 1632 events from n=12 cells, 3 mice per group) from CA3 Pyramidal neurons. (g) Schematic showing how abLIM3 knockdown in DGCs increases number of MFT filopodial contacts with PV SLINs to exert increased inhibition onto CA3 (*left*) with representative recording traces from each set of recordings (*right*). (h) Images showing PV+ puncta (arrows) in CA3 stratum pyramidale of lentiviral shNT and shRNA injected mice (*left*) and bar graph of PV puncta density in CA3 of shRNA/shNT injected mice (*right*) (two tailed unpaired t test, $^{**}p < 0.01$, n=4,4 mice, Data are represented mean ± SEM). Scale bar represents 100 μm in a and c, 10 μm in a and h, and 5 μm in c. See supplementary Table 1.

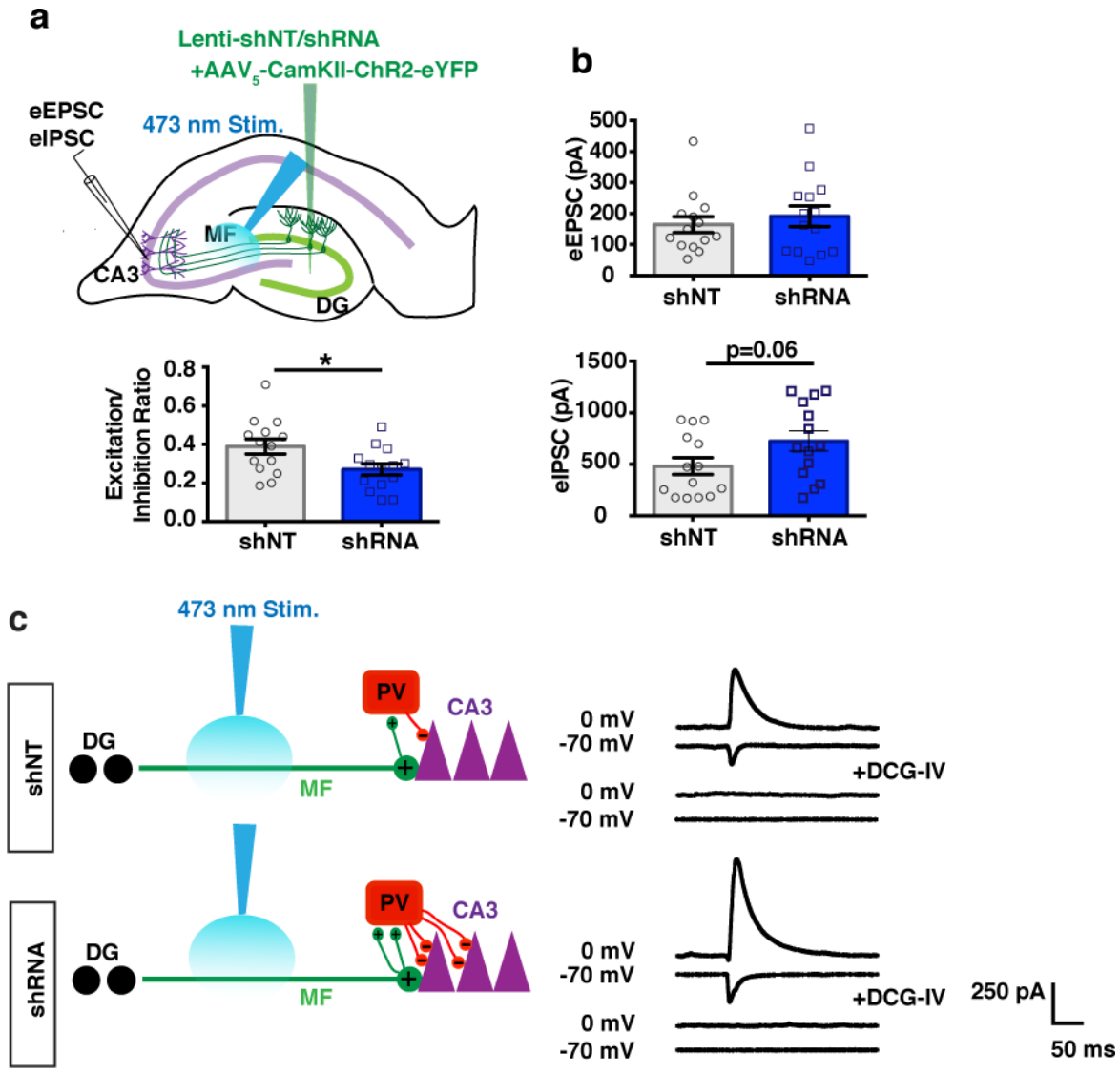

Figure 3. abLIM3 downregulation in DGCs enhances feedforward inhibition onto CA3

(a) Schematic showing lentiviral-shNT/shRNA and rAAV$_5$ CaMKIIα::ChR2–eYFP injections into DG and recording of blue light-evoked EPSCs and IPSCs in CA3 pyramidal neurons in slices (upper). Bar graph of E/I ratio (peak EPSC amplitude/peak IPSC amplitude) in CA3 of lentiviral-shRNA/shNT injected mice upon blue light stimulation (n=14 cells, 4 mice per group) (lower). (b) Absolute values of light-evoked EPSCs (upper) and IPSCs (lower) from CA3 following blue light stimulation. (c) Schematic showing how abLIM3 knockdown in DGCs increases number of MFT filopodial contacts with PV SLINs to increase feed forward inhibition onto CA3 (left) with representative recording traces from each set of recordings and traces of the same cells after perfusion of DCG-IV (right). Statistical comparisons were performed using two tailed unpaired t test, *p < 0.05, Data are represented mean ± SEM. See supplementary Table 1

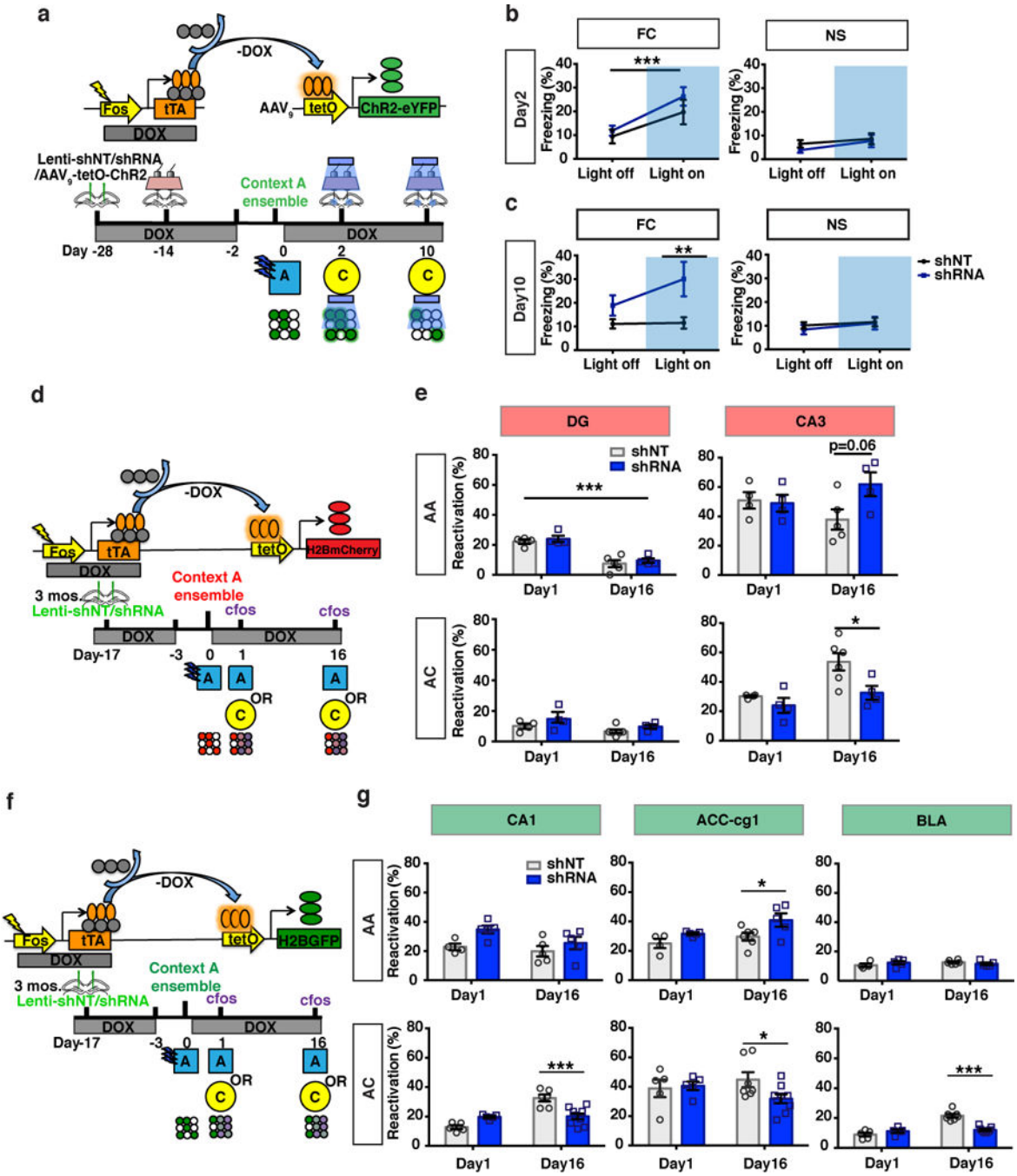

Figure 4. Enhancing DGC recruitment of inhibition promotes engram maintenance and governs reactivation of remote memory traces in hippocampal-cortical and BLA networks

(a) Schematic of virus mediated ensemble labeling strategy and behavioral paradigm for optogenetic activation of DG engram cells. (b) Freezing levels following blue light stimulation at day 2 in FC and NS groups (FC, fear conditioned, n=8,7 mice; NS, no shock, n=7,9 mice). (c) Freezing levels following blue light stimulation at day 10 in FC and NS groups [FC group:Two-way ANOVA with repeated measures, main effect of treatment (shRNA vs. shNT virus), F (1, 13) = 6.090, p=0.0283, Bonferroni post hoc, light on, p=0.0097]. (d, f) Schematic of Tet-off (Tet-Tag) genetic system and behavioral paradigm to

indelibly label ensembles in DG, CA3, CA1, BLA and ACC. (e, g) Reactivation assessed by quantifying percentage of tagged neuronal ensembles (e, tetOH2BmCherry; g, tetOH2BGFP) that are cfos+. Reactivation in AA group in DG, Two-way ANOVA, main effect of time: $p<0.001$. Reactivation in AC group: CA3, Two-way ANOVA, main effect of treatment (shRNA vs. shNT virus), $F(1, 14) = 6.972$, $p=0.019$, Bonferroni post hoc, $p=0.01$; CA1 Two-way ANOVA, day X treatment (shRNA vs. shNT virus), $F(1, 21) = 23.27$, $p<0.001$, Bonferroni post hoc, $p=0.0002$; ACC-Cg1, Two-way ANOVA, day X treatment (shRNA vs. shNT virus), $F(1, 22) = 4.318$, $p=0.04$, Bonferroni post hoc, $p=0.01$; BLA, Two-way ANOVA, day X treatment (shRNA vs. shNT virus), $F(1, 22) = 32.32$, $p < 0.0001$, Bonferroni post hoc, $p < 0.0001$, Day 1 vs. Day 16, shNT group, Bonferroni post hoc, $p<0.0001$, Day 1 vs. Day 16, shRNA group, Bonferroni post hoc, $p>0.999$. ***$p < 0.001$, **$p < 0.01$, *$p < 0.05$. Data are represented mean ± SEM. See supplementary Table 1

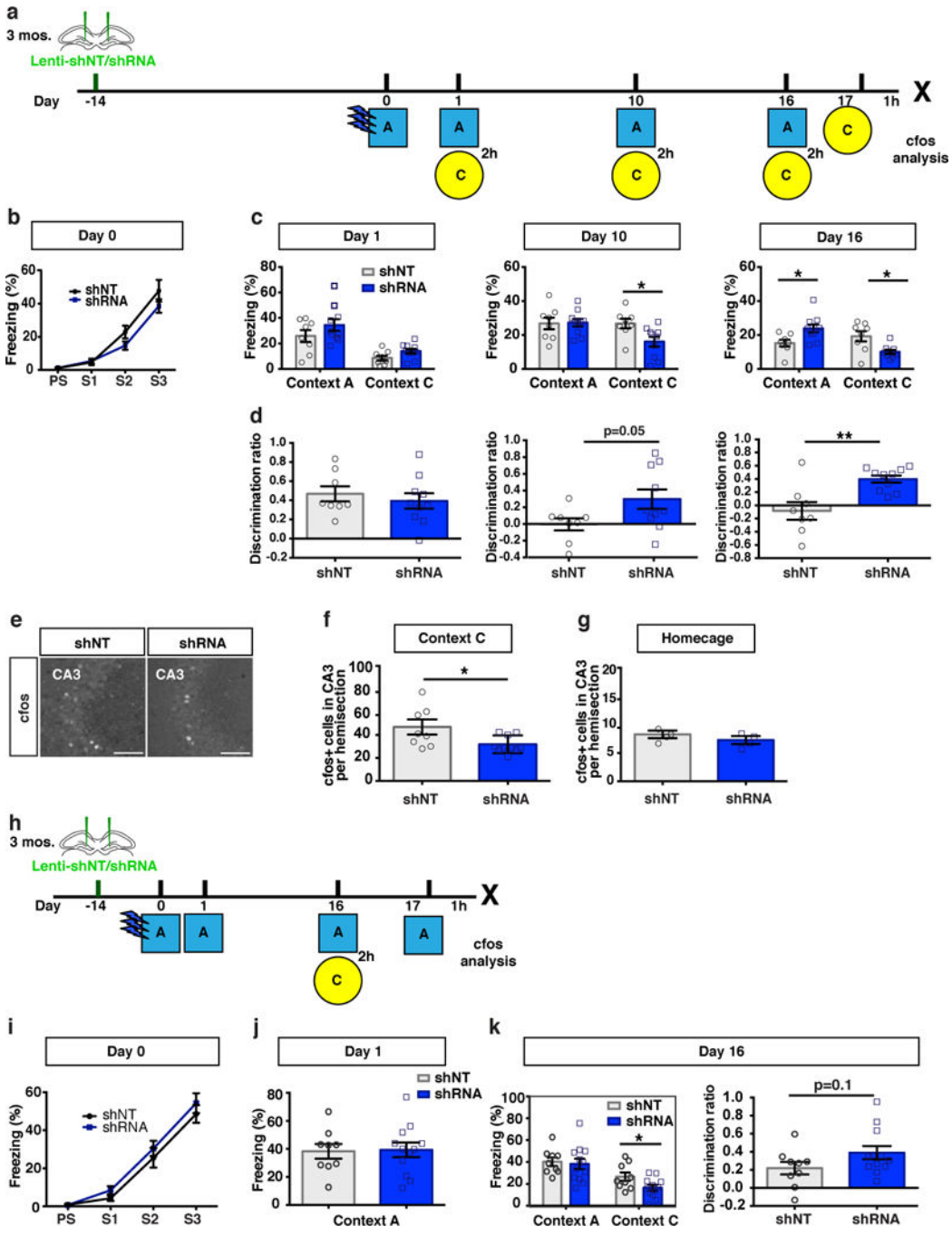

Figure 5. abLIM3 downregulation in DGCs decreases generalization of remote fear memories

(a) Schematic of contextual fear conditioning paradigm with intervening context exposures. (b) Freezing levels of lentiviral shNT/shRNA injected mice during training (n=8,10 mice, Two-way ANOVA with repeated measures). (c) Freezing levels during exposure to context A and context C at day 1, day 10 and day 16 respectively (n=8,10 mice). Two-way ANOVA with repeated measures, context X virus (shRNA vs. shNT): day 10, $F(1, 16) = 3.409$, $p=0.08$, two tailed unpaired t-test $p=0.01$; day 16, context X virus (shRNA vs. shNT): $F(1, 16) = 21.81$, $p=0.0003$, Bonferroni post hoc, $p<0.05$). Time dependent fear generalization,

one-way ANOVA with repeated measures, shNT group in context C: time, p=0.0008. (d) Contextual discrimination ratios (A *vs* C) for day 1, day 10 and day 16 (n=8,10 mice). Two-way ANOVA with repeated measures analysis of discrimination ratios, Virus X Day, F (2, 32) = 4.815, p=0.014. (e) Representative images showing cfos+ population in CA3 following lentiviral shNT/shRNA injection (*left*). (f) cfos+ cell counts after context C exposure at day 17 (n=8,10 mice). (g) cfos+ cell counts in CA3 from homecage control (n=4,4 mice). (h) Schematic of contextual fear conditioning paradigm with exposure to neutral context only at remote time point. (i) Freezing level of lentiviral-shNT/shRNA injected mice during training (n=9,12 mice, Two-way ANOVA with repeated measures). (j) Freezing level tested at day 1 and (k) day 16 (*left*) and contextual discrimination ratio (*right*) for day 16 (n=9,12 mice). Scale bar represents 100 μm. Unless otherwise specified, statistical comparisons were performed using two tailed unpaired t-tests. ***p < 0.001, **p < 0.01, *p < 0.05. Data are represented mean ± SEM. See supplementary Table 1

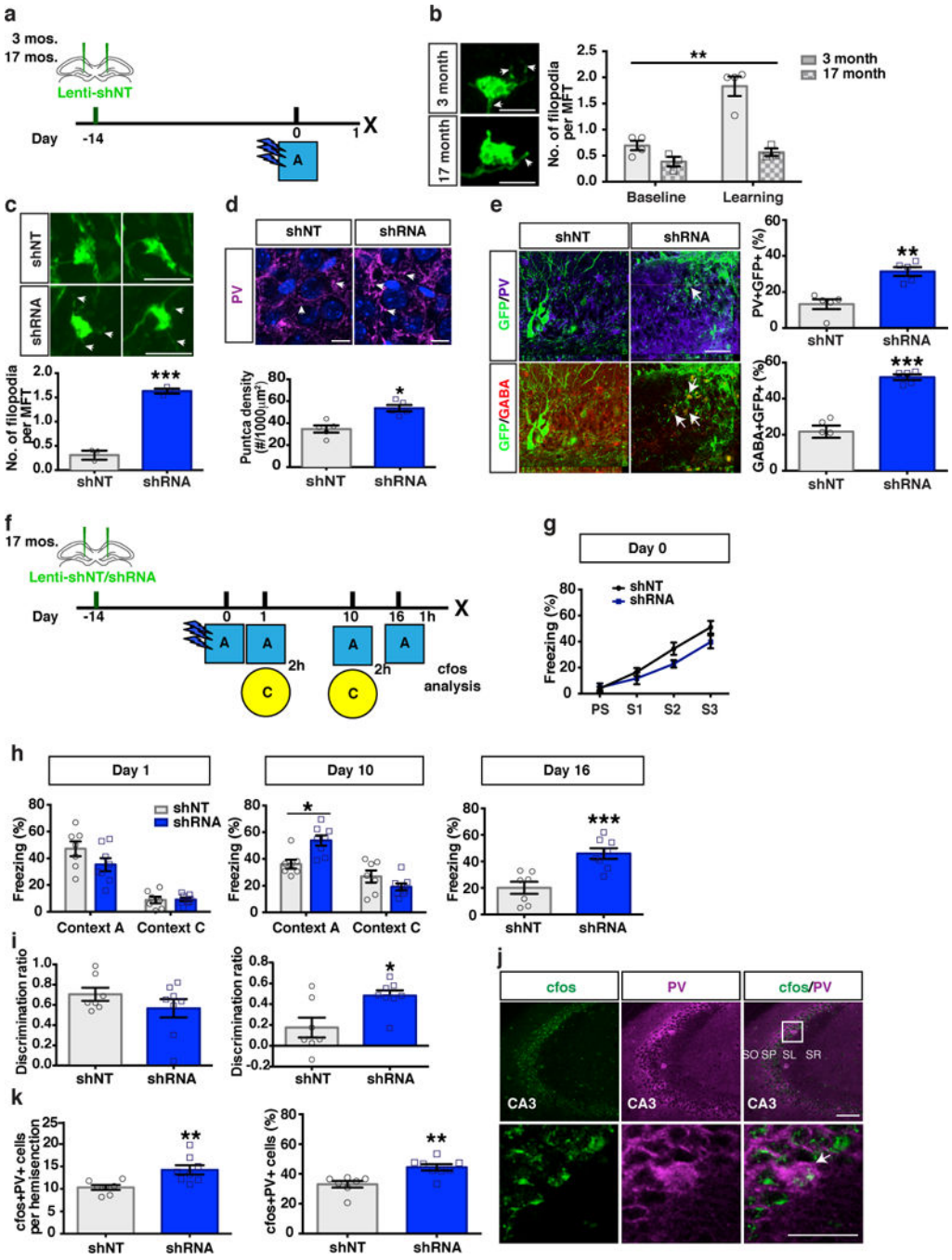

Figure 6. abLIM3 downregulation in DG of aged mice enhances DGC-PV SLIN connectivity and improves remote memory precision

(a) Schematic of lentiviral shNT/RNA injection into DG of 3-month old and 17-month old mice. (b) Representative images showing GFP+ MFTs with filopodial extensions (arrows) after training (*left*). Bar graph (*right*) showing quantification of MFT filopodia number in 3-month old and 17-month old mice at baseline (naïve, unpaired t-test, baseline, 3 month vs 17 month: p=0.06) and after training (Two-Way ANOVA, age X baseline/learning F (1, 10) = 13.03, P = 0.0048, Bonferroni's post hoc tests: 3 month, baseline vs. learning, p=0.0001. 3 month vs. 17 month following learning, p=0.0001, (4, 3 mice). (c) Representative images

(*upper*) and quantification (*lower*) showing GFP+ MFT filopodia (arrows) number (75 MFTs from shNT group and 97 MFTs from shRNA group, n=3,3 mice) following lentiviral-shNT/shRNA injection into DG of 17 months old mice. (d) Representative images (*upper*) and quantification (*lower*) showing PV puncta (arrows) density in CA3 stratum pyramidale of 17 months old mice (n=5,5 mice). (e) Representative images (*left*) and quantification (*right*) showing anterograde labeled PV and GABA+ cells in CA3 by VSV-G injection into DG of 17 months old mice (n=5,5 mice). (f) Schematic of contextual fear conditioning paradigm using aged mice. (g-h) Freezing levels of lenti-shNT/shRNA injected mice during training, test at day 1, day 10 and day 16 (n=7,8 mice). Two-way ANOVA with repeated measures (day 10), context X treatment (shRNA vs. shNT virus), $F(1, 13) = 15.58$, $p=0.0017$. (i) Contextual discrimination ratios for day 1 and day 10 (Paired t-test, Day1 vs. Day 10, in shNT mice, $p=0.0017$) (n=7,8 mice). Two-way ANOVA with repeated measures analysis of discrimination ratios, Virus X Day, $F(1, 13) = 10.74$, $p=0.006$. (j) Confocal images show cfos+PV+ cells in CA3 area [including Stratum Pyramidale (SP), Stratum Oriens (SO) Stratum Radiatum (SR) and Stratum Lucidum (SL)]. After context A exposure at day 16. (k) Bar graph with quantification of cfos+PV+ cells counts (*left*) and percentage of cfos+PV+ cells over total PV+ cells in CA3 area (*right*) (n=7,8 mice). Scale bar represents 100 μm in j, 50 μm in e and j, 10 μm in d, 5 μm in b and c. Unless otherwise specified, statistical comparisons were performed using two tailed unpaired t-tests. ***$p < 0.001$, **$p < 0.01$, *$p < 0.05$. Data are represented mean ± SEM. See supplementary Table 1